Molecular symmetry group analysis of the low-wavenumber torsions and vibration-torsions in the S_1 state and ground state cation of *p*-xylene: an investigation using resonance-enhanced multiphoton ionization (REMPI) and zero-kinetic-energy (ZEKE) spectroscopy

Adrian M. Gardner,[a] William D. Tuttle,[a] Peter Groner,[b,c] and Timothy G. Wright[a,d]

[a] School of Chemistry, University of Nottingham, University Park, Nottingham NG7 2RD UK

[b] Department of Chemistry, University of Missouri - Kansas City, Kansas City, MO 64110, USA

[c] Email: GronerP@umkc.edu

[d] Email: Tim.Wright@nottingham.ac.uk

Abstract

For the first time, a molecular symmetry group (MSG) analysis has been undertaken in the investigation of the electronic spectroscopy of *p*-xylene (*p*-dimethylbenzene). Torsional and vibration-torsional (vibtor) levels in the S_1 state and ground state of the cation of *p*-xylene (*p*-dimethylbenzene) are investigated using resonance-enhanced multiphoton ionization (REMPI) and zero-kinetic-energy (ZEKE) spectroscopy. In the present work, we concentrate on the 0–350 cm^{-1} region, where there are a number of torsional and vibtor bands and we discuss the assignment of this region. In an accompanying paper [Tuttle et al. J. Chem. Phys. XXX, xxxxxx (2016)], we examine the 350–600 cm^{-1} region where vibtor levels are observed as part of a Fermi resonance. The similarity of much of the observed spectral activity to that in the related substituted benzenes, toluene and *para*-fluorotoluene, is striking, despite the different symmetries. The discussion necessitates a consideration of the MSG of *p*-xylene, which has been designated G_{72}, but we shall also designate [3,3]D_{2h} and we include the symmetry operations, character table and direct product table for this. We also discuss the symmetries of the internal rotor (torsional) levels and the selection rules for the particular electronic transition of *p*-xylene investigated here.

I. INTRODUCTION

The prevalence of molecules that contain methyl groups, and their role in understanding photophysical phenomena, has led to fundamental studies on simple molecules. The body of work from the group of Parmenter and coworkers (see Ref. 1 and other work by the same group) is noteworthy, where a significant amount of work has been undertaken comparing the molecules *p*-difluorobenzene (*p*DFB) and *p*-fluorotoluene (*p*FT). This work has been given a modern twist by the group of Reid using time-resolved photoelectron spectroscopy (tr-PES) (see Ref. 2 and other work by the same group), with whom we have collaborated.[3,4]

In previous work, our group has studied toluene, using resonance-enhanced multiphoton ionization (REMPI) and zero-kinetic-energy (ZEKE) spectroscopy,[5,6] as has the group of Lawrance,[7] using two-dimensional laser-induced fluorescence (2D-LIF). Recently, this work was furthered by Lawrance and coworkers,[8,9] with the role of methyl groups in coupling to vibrational levels being emphasised. This is related to the concept of intramolecular vibrational redistribution (IVR), or more generally intramolecular energy redistribution. These coupling processes are important since they can govern the rapid dispersal of internal energy within a molecule following photoexcitation, giving it enhanced photostability – particularly pertinent to biomolecules.[10,11] Thus, an understanding of the role of torsions in such mechanisms requires knowledge of the torsional and vibration-torsional (vibtor) level structure in different molecules. In particular, the assignment of the vibrations (atomic motion) will underpin models of how interactions with torsional motion occurs. In previous work, our group has also studied the *p*FT molecule;[4,12,13] as has the group of Lawrance,[14,15] some of which was in collaboration with ourselves. In addition, we shall make passing comment on previous fluorescence work on *p*FT,[16,17,18] ZEKE spectroscopy on toluene by Lu et al.[19] and ZEKE spectroscopy on *p*FT by Takazawa et al.[20] and ourselves.[12,13]

In the present work, we examine the $S_1 \leftarrow S_0$ electronic transition in *p*-xylene (*p*Xyl), which has two methyl groups that are located on opposite sides of a phenyl ring, using REMPI and ZEKE spectroscopy. We shall discuss the 0–350 cm^{-1} region in detail, guided by the above-cited previous work on toluene and *p*FT, in terms of both transitions between internal rotor levels in the two states, and those involving interactions between low-lying vibrational and torsional levels – the vibtor levels mentioned above. We shall initially remark on the similarity

of the structure < 100 cm^{-1} that arises from the "pure" torsional bands for toluene, *p*FT and *p*Xyl, then further remark on how similar the structure is up to 200 cm^{-1} for *p*FT and *p*Xyl, which is attributable to torsional and vibtor bands. These similarities, and the departure therefrom for the structure above 200 cm^{-1}, will be noted and discussed.

As noted in ref. 9, vibration-torsional interactions will pervade the higher energy levels of each electronic state and so combination levels involving such vibtor levels must be considered when assigning the rest of the spectrum. In an accompanying paper, we shall consider the 350–600 cm^{-1} region of the spectrum of *p*Xyl, where it will be seen that, although dominated by vibrational bands, vibtor levels also appear in this region.[21]

We note that other workers have studied the electronic spectrum of *p*Xyl .[22,23,24,25,26,27,28,29,30] There have also been studies on the cation that have involved intermediate vibronic excitation steps: REMPI combined with photoelectron spectroscopy (REMPI-PES)[25]; ZEKE spectroscopy;[31] and mass-analyzed threshold ionization (MATI) spectroscopic studies.[28,29,32] The latter studies have a much higher resolution than both an earlier photoionization study,[33] and HeI photoelectron work that at best only showed partially-resolved and unassigned vibrational bands.[34,35,36,37] We shall only discuss pertinent aspects of the previous studies at appropriate points of the present paper.

II. THEORETICAL BACKGROUND

A. Single rotor

Molecules containing methyl groups undergo some internal motions that may be considered as torsions. These are also often termed (hindered) internal rotations and these terms are used largely interchangeably in the literature, depending on the context and emphasis. In Appendix A we outline the key points regarding the energy levels and labelling of single-rotor molecules[38] such as toluene[39,40] and *p*FT, which belong to the G_{12} molecular symmetry group (MSG).[41,42] (The atom numbering is presented in Figure 1.) In particular, we provide the rationale as to why, even under jet-cooled conditions such as used in the present work, both the m = 0 and m = 1 torsional levels are populated. These ideas underpin those for a two-rotor system – the focus of the present work – which is developed in the next subsection.

B. Two-rotor systems

1. Background and Previous Work

Although there has been a wealth of detailed studies on the spectroscopy of molecules with two methyl rotors,[38,41] this has largely been concentrated on microwave spectroscopy and as such the *p*Xyl molecule has received little attention, since it has no permanent dipole moment. That said, there also seem to have been no detailed infrared studies of *p*Xyl examining the torsional levels, although there have been such studies for other dimethyl molecules.[43,44] For non-centrosymmetric molecules, many articles are available that cover the background theory of such systems, sometimes alongside a description of a computational program (see Groner[45] for a recent review of these). In principle, the detailed theory required to study the energy levels in *p*Xyl is available, in papers such as that by Swalen and Costain,[46] Groner and Durig[43] and books such as that by Wollrab[38] and the key treatise in the area by Bunker and Jensen[41] (see also ref. 42), but we are unaware of any detailed development and application of the theory to a specific analysis of the spectroscopy of *p*-xylene.

We note that Breen et al.[23] have studied the $S_1 \leftarrow S_0$ electronic transition in the three different xylenes and considered (in overview) the effect of the two rotors in discussing the assignment of their spectrum. They concluded that, at their resolution, the methyl rotors are essentially non-interacting, and this was expected to be particularly true for *p*Xyl where they are the most distant. Although noting that the true levels would have a definite symmetry in the full MSG for *p*Xyl, Breen et al.[23] assigned the structure seen in the case of *p*Xyl in terms of the same levels as seen in the single-rotor case, toluene; however, they assigned some levels in terms of independent excitation of each methyl group. We make two comments on this assignment: first, the *p*Xyl torsional levels will in fact each correspond to linear combinations of the single-rotor levels, in order to be of a definite symmetry in the MSG of *p*Xyl; and secondly, as we shall see below, the expected intensities and also comparison of the present work with the corresponding spectrum of *p*FT, implies that some of the previous assignments for *p*Xyl are incorrect.

2. Axis systems

We define the axis systems employed, in Figure 2, with the numbering given in Figure 1. For benzene, the molecule lies in the *xy* plane, with the *z* axis coincident with the C_6 symmetry axis. For a D_{2h} molecule, the *z* axis will pass through the fluorine atoms of *p*DFB, but the protocol for selecting the *x* and *y* axes are not so definitive. We follow the axis system employed by Knight and Kable,[47] who located the molecule in the *yz* plane. (A similar issue arises with a C_{2v} molecule and, where discussed, to be consistent with our previous work, we also locate the molecule in the *yz* plane, with the *z* axis passing through the unique substituent atom (or group) and the centre of the phenyl ring.) With these axis conventions, in the D_{6h} point group for benzene, the S_1 state is designated $\tilde{A}^1B_{2u}$, the S_2 state is $\tilde{B}^1B_{1u}$, and the S_3 state is $\tilde{C}^1E_{1u}$. These will be pertinent to a discussion of Herzberg-Teller (HT) vibronic coupling effects that will be presented later. For the G_{12} MSG, the *a* axis (coincident with the *z* axis) passes through the *ipso* and *para* carbon atoms of the phenyl ring as well as the carbon of the methyl group, and the phenyl ring lies in the *ab* (*yz*) plane; the *c* (*x*) axis is thus perpendicular to the phenyl ring.

3. Molecular symmetry group of p-xylene

The MSG of *p*Xyl is of order 72[43] and has been referred to as G_{72}, but it does not yet appear to have been applied to its spectroscopy. It has been mentioned in the literature, such as in the paper by Groner and Durig[43] (where it was denoted $\theta_3 \times \theta_3 \times V_2$ or $C_{3v}T–D_{2h}F–C_{3v}T$, where the *T* refers to the CH_3 groups (torsions), and the *F* to the framework to which these are attached); additionally, some guidance as to the construction of the G_{72} character table has been given.[41,48,49] We also note that Smeyers and coworkers have considered symmetry effects on the potential energy and conformational behaviour of two-rotor (and higher-rotor) molecules.[50,51,52,53]

Most molecular symmetry analyses begin with the PI operators of feasible motions to derive the commutation relations between the operators and to establish the MSG and its character table. It is then possible to determine Γ^*, the irreducible representation dictating the selection rules for electric dipole transitions and to reduce the representation of the nuclear spin functions. The description of everything else in spectroscopic problems requires the definition of rotational and internal (large-amplitude and vibrational) coordinates. We begin with the

definition of the nuclear position vectors as functions of Eulerian angles and internal coordinates and determine the substitutions of the coordinates and that lead to permutation-inversion (PI) operators of feasible motions. Hence, to derive the MSG of *p*Xyl, the molecule is placed into a molecule-fixed Cartesian (frame) axis system. In this axis system, see Figure 1(b), the frame position vectors of the H atoms in the phenyl group are given by:

$$X_{jl}^{f} = D(l\pi, j\pi, 0)\, D(0, \varphi, 0)\, R_H\ , \qquad l, j = 1, 2 \tag{1}$$

While the positions of the methyl group H atoms are defined as:

$$X_{jk}^{f} = D(j\pi, j\pi, 0)\left[R + D\left(\tau_j + k\omega, \theta, 0\right) R_X\right]$$

$$\omega = (2\pi)/3, \qquad j = 1, 2; \qquad k = 0, 1, 2 \text{ (modulo 3)} \tag{2}$$

R_H, R and R_X are vectors whose *b*- and *c*-components are zero; the *a*-components are the distances of: a phenyl H atom from the origin; a methyl C-atom from the origin; and a methyl H atom from its corresponding methyl C atom, respectively. (The position vectors of the C atoms are not required to derive the symmetry operators, since they can be inferred from those of the H atoms; their positions can be found by replacing R_H by R_C in Eq. (1), which generates the position vectors of the C atoms a, b, c, and d; further, setting R_X to the null vector in eq. (2) defines the locations of the methyl C atoms; and changing R to R' in that last expression generates the positions of the *ipso* and *para* phenyl C atoms.) The rotation matrices *D* are defined according to:

$$D(\alpha, \beta, \gamma) = D(\alpha, 0, 0)\, D(0, \beta, 0)\, D(0, 0, \gamma)$$

$$= \begin{pmatrix} \cos\alpha & -\sin\alpha & 0 \\ \sin\alpha & \cos\alpha & 0 \\ 0 & 0 & 1 \end{pmatrix} \begin{pmatrix} \cos\beta & 0 & \sin\beta \\ 0 & 1 & 0 \\ -\sin\beta & 0 & \cos\beta \end{pmatrix} \begin{pmatrix} \cos\gamma & -\sin\gamma & 0 \\ \sin\gamma & \cos\gamma & 0 \\ 0 & 0 & 1 \end{pmatrix} \tag{3}$$

In the space-fixed axes system, the Cartesian coordinate vectors are given by:

$$X_{jm} = D(\alpha, \beta, \gamma)\, X_{jm}^{f}$$

(4)

Where α, β and γ are the Eulerian angles defining the rotation of the molecule in space. The S^{-1} matrix that is used by many (see, for example, Hougen)[44,54] is related to the D matrix as follows:

$$S^{-1}(\chi,\theta,\varphi) = D(\varphi,\theta,\chi)$$

(5)

It is easy to show that the five generating operators C_1, C_2, D, S and T, which are defined in Tables I and II, are symmetry operations which lead to permuted position vectors and corresponding PI operators. (Note that S and D have also been used for rotation matrices above – the context makes it clear to what we are referring in each case.) All the generating operators commute with each other, except for:

$[S,C_j] = C_j^{-1}$, and $[T,C_j] = C_{3-j}$

(6)

Specifically, D commutes with any of the other operators C_j, S, and T. The molecular symmetry group can therefore be denoted $[3,3]D_{2h} = [3,3]C_{2v} \times \{E, D\}$. In this notation,[55] $[3,3]G$ stands for the semidirect product $(C_3 \times C_3) \wedge G$, where C_3 is the cyclic group of order 3; $\times$ and $\wedge$ are the symbols for a direct product and semidirect product, respectively; and G is the symbol for a point group. $\{E, D\}$ is the group of order 2 containing the elements E and D. The group $[3,3]C_{2v}$ has been called $C_{3v}^- \times C_{3v}^+$ in some work,[56,57] $\theta_3 \times \theta_3$ in others,[43,58] and G_{36} in some publications on acetone-like molecules.[59] While the PI groups, each denoted G_{36}, for acetone and dimethylacetylene are isomorphic their application to vibronic states[59] necessitates the extended PI group $G_{36}^{\dagger} = G_{72}$ "double group" for dimethylacetylene, but not for acetone. In fact, $[3,3]D_{2h}$ for *p*Xyl is isomorphic to G_{72} but, in this case, it is not a "double group".

The character table of $[3,3]D_{2h}$ is given in Table III. The labels of the $[3,3]D_{2h}$ irreducible representations consist of the two symmetry numbers σ_1 and σ_2 for each of the individual internal rotors. To this are appended a g or u subscript for positive or negative character under operator D and superscripted signs s_1 and s_2, which represent the behaviour under T and/or U (=TS), respectively, as follows: for 00 levels both signs will be present (both

characters are ±1); for 11 levels there will be a single sign, s_1 (the character of T is ±2, while that for U is 0); for 12 levels there will be a single sign, s_2 (the character of U is ±2, while that for T is 0); and for 01 levels there will be no such sign (both characters are 0).

Also, included in Table III is a column that contains irreducible representation labels that are based on the labels of G_{36} in ref. 41, since $G_{72} = G_{36} \times \{E, D\}$; we shall use these "$G_{72}$" labels when discussing the assignment of the spectra later on. The PI operators of G_{72} are identified with those of [3,3]D_{2h} in Table II.

The transformation properties of the free internal rotor functions

$$|m_1 m_2\rangle = (2\pi)^{-1}\, e^{im_1\tau_1} e^{im_2\tau_2}\,, \quad 0 \le \text{integers } |m_1|, |m_2| < \infty \tag{7}$$

are shown in Table IV. The symmetry operators T, U, and S transform the functions $|m_1 m_2\rangle$ into $|m_2 m_1\rangle$, $|{-m_2}{-m_1}\rangle$ and $|{-m_1}{-m_2}\rangle$, respectively. The set of these four functions is labelled by $\{m_1, m_2\}$. When $|m_1| = |m_2|$, the set contains only two functions, and for $|m_1| = |m_2| = 0$, the set has only one function. In Table IV, m_1 and m_2 have been expressed with the symmetry numbers as:

$$m_1 = 3m+\sigma_1 \quad \text{and} \quad m_2 = 3n+\sigma_2$$

$$\sigma_1 = m_1 \text{ (modulo 3)} \quad \text{and} \quad \sigma_2 = m_2 \text{ (modulo 3)} \tag{8}$$

The appropriate linear combinations for each irreducible representation are given in Table V.

The symmetry characteristics of the rotational basis functions are derived from their properties in the molecular symmetry group [3,3]D_{2h}. Since *p*Xyl is an asymmetric rotor, we can express them in terms of the parities (*e* for even, *o* for odd) of the K_aK_c labels of an asymmetric rotor. Functions with parities *ee*, *eo*, *oo* and *oe* transform like 00_g^{++} (A_1'), 00_g^{-+} (A_2'), 00_u^{+-} (A_3''), and 00_u^{--} (A_4''), respectively. The electric dipole moment is of course a function of the internal rotation angles τ_1 and τ_2. The transformation properties of the simplest periodic functions are listed in Table VI for G_{72} and will be made use of later.

4. Nuclear Spin States and Jet Cooling

In Appendix A, we outline why it is that even under the coldest jet-cooled conditions, we still expect significant populations in the m = 0 and m = 1 torsional levels for a single-rotor system, because of satisfying the Pauli principle when nuclear spin states are considered. A similar situation arises in the case of *p*Xyl, and this is developed in Appendix B. The conclusion is that now we expect four torsional levels to be populated under jet-cooled conditions: {0,0}, {0,1}, {1,1} and {1,-1}. As a consequence, excitations from $S_1 \leftarrow S_0$ can involve any of these four levels.

5. Labelling the {m_1,m_2} states

Because of the degeneracies of the various levels, a single {m_1, m_2} label can be used for various combinations of pairs of m_i, m_j quantum numbers (see Tables IV and V, discussion above and Appendix C.) In addition, to be able to compare assignments between one-rotor and two-rotor systems, it will prove useful to have alternative labels for the {0, m} states for m = 0 modulo 3 ($m \neq 0$) levels. These are $\{0,3(+)\}^+$ and $\{0,3(+)\}^-$ and $\{0,3(-)\}^+$ and $\{0,3(-)\}^-$, which are +/- combinations of the m = 3(+) and m = 3(-) levels on each rotor – see Appendix C.

6. Hamiltonian for coupled equivalent internal rotors

As usual, the Hamiltonian is the sum of operators for the kinetic energy, T, and the potential energy, V:

$$H = T + V \tag{9}$$

The kinetic energy for a two-rotor system, without the contributions from the coupling with overall rotation, may be written as (see Eq. (5c) in ref. 60)

$$T = \begin{pmatrix} p_1^* & p_2^* \end{pmatrix} \begin{pmatrix} F & F' \\ F' & F \end{pmatrix} \begin{pmatrix} p_1 \\ p_2 \end{pmatrix}$$

(10)

The symbols p_j and p_j^* represent the internal angular momentum operator for rotor *j* and its complex conjugate, respectively. For methyl internal rotors, the quantities *F* and *F′* are essentially constant and are obtained from:

$$F = (I_a - I')\, d$$

$$F' = -I'd$$

$$d = (h/8\pi^2 c)/[I'(I_a - 2I')]$$

(11)

where I_a is the smallest principal moment of inertia for overall rotation of the whole molecule and I' is the moment of inertia of one methyl group about its internal rotation axis. Approximate values of these parameters, obtained from calculated equilibrium ("R_e") structures from B3LYP/aug-cc-pVTZ and TD-B3LYP/aug-cc-pVTZ optimized structures of *p*Xyl[21] are (in cm^{-1}), F = 5.591 and F' = -0.194 for the S_0 state and F = 5.547 and F' = -0.184 for S_1. Neglecting higher orders in the internal angular momenta, the kinetic energy is then given by

$$T = F\,(p_1^2 + p_2^2) + 2F'p_1p_2$$

(12)

The potential function can be written as a 2-dimensional Fourier series

$$2V(\tau_1, \tau_2) = \sum_{j,k} V_{j,k}\; e^{ij\tau_1} e^{ik\tau_2}$$

(13)

The generating symmetry operators C_1 and C_2 (see Tables I and II) require that *j* and *k* are signed integer multiples of 3. The other generating operators of Table II, together with the condition that $V(\tau_1, \tau_2)$ be real, lead to the following relations between the coefficients, $V_{j,k}$:

$$V_{j,k} = V_{j,k}(-1)^{j+k} = V^*_{-j,-k} = V_{-j,-k} = V_{k,j} = V_{-k,-j}$$

(14)

These relations also mean that the coefficients, $V_{j,k}$, are real and, moreover, that they may be non-zero only for *j*+*k* = even. Therefore, the potential function may be rewritten:

$$2V(\tau_1,\tau_2) = V_{0,0} + 2\sum_{j=3,3}\left[V_{j,j}\cos\left(j(\tau_1+\tau_2)\right) + V_{j,-j}\cos\left(j(\tau_1-\tau_2)\right)\right]$$

$$+2\sum_{j=6,3}\ \sum_{k=-j+6,6}^{j-6} V_{j,k}[\cos(j\tau_1+k\tau_2)+\cos(k\tau_1+j\tau_2)]$$

(15)

In this equation, the summation index *j* increases in steps of 3 whereas *k* increases in steps of 6. Besides the trivial constant, $V_{0,0}$, the lowest order coefficients in this potential function are $V_{3,3}$, $V_{3,-3}$ and $V_{6,0}$. A simplified expression may therefore be written:

$$V(\tau_1,\tau_2) = \left(V_{3,3}+V_{3,-3}\right)\cos 3\tau_1\cos 3\tau_2$$

$$-\left(V_{3,3}-V_{3,-3}\right)\sin 3\tau_1\sin 3\tau_2 + V_{6,0}\left(\cos 6\tau_1+\cos 6\tau_2\right)$$

(16)

A potential function described by this equation with a dominant $V_{6,0}$ coefficient has 36 minima and 36 maxima over a range of 2π of both variables. The minima and maxima (which occur in pairs) in the $-\pi/3 < \tau_1, \tau_2 \le \pi/3$ range are listed in Table VII for $V_{6,0} > 0$, together with their energies and descriptions. The energy minima occur for conformations in which one C-H bond of each methyl group are in the *ac* plane (the methyl groups are staggered (ss) with respect to the benzene ring). One pair of these is labelled $C_{2h}(b)$ because it has $C_{2h}(b)$ point group symmetry with the C_2 axis coinciding with the *b* axis). The other pair of minima is labelled $C_{2v}(c)$. The structures at the maxima of the potential have one C–H bond of each methyl group eclipsing the benzene ring (ee). They are labelled $C_{2v}(b)$ or $C_{2h}(c)$. The energies of minima, maxima and saddle points are given in terms of the potential coefficients, also their relative energy with respect to conformation $C_{2h}(b)$. This structure is the one shown in Figure 1, which

is the calculated minimum energy structure in the electronic ground state S_0.[21] If the $C_{2h}(b)$ structure corresponds to the global minimum (in S_0), $V_{3,3}$ must be smaller than $V_{3,-3}$. Structure $C_{2v}(c)$ corresponds to the structure of the S_1 state. For the $C_{2v}(c)$ structure to be the global minimum (in the S_1 state), $V_{3,3}$ must be larger than $V_{3,-3}$.

Figure 3 contains contour plots of potentials which have global minima at the $C_{2h}(b)$ and C_{2v}(c) conformations. In both plots, the horizontal axis (τ_1) and vertical axis (τ_2) run from $-\pi/3$ to $+\pi/3$. The global minima and maxima of the potential are in the centre of the dark purple and dark orange areas, respectively.

The potential coefficients, $V_{3,3}$, $V_{3,-3}$ and $V_{6,0,}$ cause the first order splittings of levels that belong to the {0,3} set of free internal rotor functions. Table VIII displays the matrix with the interaction matrix elements, with the resulting energies of the symmetrized functions being given in Table IX. These results will be discussed later.

7. Vibrational Labels

In the same way that the vibrations of monosubstituted benzenes are significantly different from those of benzene,[61] the presence of a second substituent also modifies the vibrations significantly, both in form as well as wavenumber, so that they are different from those of both benzene and the monosubstituted species. We have recently examined the vibrations of *para*-disubstituted benzenes[62] and in the present work we shall use the D_i nomenclature described therein for the vibrational labels.

III. EXPERIMENTAL

The REMPI apparatus employed has been described previously in detail elsewhere,[63] with small modifications having been incorporated in order to perform the two-colour ZEKE experiments, which have also been described,[64] and so only a brief description is given here. The excitation laser was a dye laser (Sirah Cobra-Stretch) operating with C540A and was pumped with the third harmonic (355 nm) of a Surelite III Nd:YAG laser. The ionization laser was a dye laser (Sirah Cobra-Stretch) operating with DCM pumped with the second harmonic (532 nm) of a Surelite I Nd:YAG laser. The fundamental frequencies produced by each dye

laser were frequency doubled using beta-barium borate (BBO) and potassium dihydrogen phosphate (KDP) crystals for the pump and probe lasers, respectively.

The vapour above room temperature *p*-xylene (99.5% purity, Sigma-Aldrich) was seeded in ~1.5 bar of Ar and the gaseous mixture passed through a General Valve pulsed nozzle (750 μm, 10 Hz, opening time of 180–210 μs) to create a free jet expansion. The focused, frequency-doubled outputs of the two dye lasers were overlapped spatially and temporally and passed through a vacuum chamber coaxially and counterpropagating. Here they intersected the free jet expansion between two biased electrical grids located in the extraction region of a time-of-flight mass spectrometer, which was employed in the REMPI experiments. These grids were also used in the ZEKE experiments by application of pulsed voltages, giving typical fields (*F*) of ~10 V cm^{-1}, after a delay of up to 2 μs, where this delay was minimized while avoiding introducing excess noise from the prompt electron signal. Because of the well-known decay of the lower-lying Rydberg states accessed in the pulsed-field ionization process,[65] bands had widths of ~5–7 cm^{-1}, even when $\sqrt{F}$ relationships would suggest the widths should be significantly greater.

IV. RESULTS AND DISCUSSION

A. REMPI Spectrum - Overview

The 0–350 cm^{-1} region of the (1+1) REMPI spectrum of *p*Xyl is presented in Figure 4, where it is compared with the corresponding spectra of *p*FT and toluene having been previously published in Refs. 13 and 5, respectively. The spectra are presented on a relative wavenumber scale, with the wavenumbers of the origin transitions noted in the figure caption. If we treat the methyl groups as point masses, as noted above, then *p*Xyl may be considered in the D_{2h} point group, and the resulting transition may be denoted $\tilde{A}\,^1B_{2u} \leftarrow \tilde{X}^1A_g$; for molecules with C_{2v} point group symmetry, then the transition is $\tilde{A}\,^1B_2 \leftarrow \tilde{X}^1A_1$. The transition observed here for *p*Xyl is hence the corresponding transition observed in our recent REMPI work on monohalobenzenes[66,67,68] toluene,[5,6] and *p*FT[3,13] (in the latter two cases, if the methyl group is again taken to be a point mass).

As may be seen from Figure 4(c), the first ~ 350 cm^{-1} of the spectrum of *p*Xyl above the intense origin band consists of a series of weak features. The lowest wavenumber weak features have been discussed by Breen et al.[23] in terms of torsions only; but, by analogy with the recent work by Gascooke et al. on toluene,[8] and recent work by them and us on *p*FT,[13,14,15] (see also the work of Zhao[18]), we also expect some contribution from low-wavenumber vibrations via vibration-torsional coupling in this region of the spectrum. We note that Ebata et al.[22] saw very few features in this wavenumber region and indeed there were very few features in their wider-range spectrum and none below 600 cm^{-1}. In contrast, Gunzer and Grotemeyer[28,29] observed a number of low-wavenumber bands, but only assigned these to generic "methyl torsions"; a few others to higher wavenumber were assigned to vibrations using Wilson notation and a discussion of this region is contained in our accompanying paper.[21] Additionally, they observed torsional bands in their MATI spectrum, plus some unassigned features, which we shall also remark upon below. Blease et al.[24] observed a few torsional transitions, but these were only generically assigned; they also gave assignments for four of the vibrational bands in this region, again which we shall comment in the accompanying paper.[21] They noted some other features in their REMPI spectrum that were unassigned and we shall comment on some of these below. The REMPI spectrum presented in ref. 24 appears to be the best quality of those previously reported (albeit with little comment regarding the assignment therein) and is in excellent agreement with that presented in Figure 4(c) of the present work.

With regards to the cation, the resolution and/or signal-to-noise in Walter et al.'s REMPI-PES study[25] was not sufficient to see any torsional bands. Gunzer and Grotemeyer[28] observed some torsional bands in their MATI spectrum, but these were only assigned in a generic way. On the other hand, Held et al.[31] provided detailed assignments for ZEKE bands that they observed when exciting via the S_1 origin, in terms of transitions on one or both methyl groups. Similar to our comments above regarding the $S_1 \leftarrow S_0$ spectrum of Breen et al.,[23] we are not convinced that the picture presented is entirely correct for the full molecular symmetry group and indeed will reassign a number of bands later in the present paper.

In the following, we shall discuss the assignment of the main REMPI features by reference to the activity we see in the ZEKE spectra when we excite through various S_1 levels that are each

the terminating states of various REMPI transitions; we shall also find it useful to make analogy with the corresponding spectra of toluene and *p*FT.

On occasion, we were able to identify some bands in the REMPI spectra of *p*Xyl attributable to complexation of *p*Xyl with Ar via their changing relative intensities with conditions, the observation of the parent cation in the mass spectrum, and by comparison with the work of Lu et al.[69] We do not believe any of the spectra presented herein are contaminated to any significant extent by bands arising from complexes.

B. "Pure" Torsional Transitions

In Figure 4 we show the 0–350 cm^{-1} region of the REMPI spectra of toluene, *p*FT and *p*Xyl. In the case of toluene, the assignment of the region < 100 cm^{-1} has been discussed by Walker et al.[39] and more recently by Virgo et al.[40] with a particular emphasis on explaining the relative intensities of the symmetry-forbidden bands. The explanation for these was based on electronic-torsional coupling via a Fourier expansion of the transition dipole moment in terms of the torsional angle. It was deduced that the $m_0^{3(+)}$ transition should be the most intense of the non-Franck-Condon bands and other Δm = 3 transitions should be seen, explaining the presence of the m_1^2 and m_1^4 bands (noting that *m* can be signed). This explanation did not, however, explain the appearance of the very weak $m_0^{3(-)}$ transition, which was suggested as arising from torsion-rotation coupling, with this considered in detail by Virgo et al.,[40] where simulations gave close-to-quantitative agreement with experiment, and revealed the dependence of the intensity of the $m_0^{3(-)}$ feature on the magnitude of V_6 and the rotational temperature. (Here the m_a^b notation indicates a transition from *m* = *a* in the S_0 state to *m* = *b* in the S_1 state.)

The assignment of the spectrum of toluene was largely confirmed by ZEKE experiments[19] based upon expected selection rules and the more general analogue of the Δv = 0 vibrational propensity rule, which we designate the "$\Delta(v,m)$ = 0" propensity rule, referring to preferential excitation of the same vibrational and torsional character in the cation as in the intermediate S_1 level. In ref. 9, Gascooke et al. showed that essentially the same assignment of the torsional features in the $S_1 \leftarrow S_0$ transition resulted when considering vibration-torsion coupled levels, but that the values of the effective rotational constants and V_6 barrier heights were different

– very starkly so for V_6. In the absence of any significant perturbation of the potential by the presence of the fluorine atom in *p*FT, and with the comments above concerning the excitation of the non-interacting methyl torsions in *p*Xyl, we would expect the appearance of the REMPI spectra for the three molecules, toluene, *p*FT and *p*Xyl to be very similar in this region. In fact, as may be seen from Figure 4, the regions < 100 cm^{-1} do indeed look very similar in all three spectra, indicating that the assignments are expected to correspond. It is then noteworthy that also in the region 100–200 cm^{-1}, the spectra of *p*FT and *p*Xyl agree very closely, while that of toluene is somewhat different; in the below, we shall attribute this to an almost identical value of D_{20} in the S_1 state of *p*FT and *p*Xyl, while the value of the lowest wavenumber vibration in toluene is somewhat different. In the region 200–350 cm^{-1} it may be seen that the spectra of *p*FT and *p*Xyl now also differ – this will be attributed to the different value of D_{19} in the S_1 state of the two molecules. (Note from Refs 13 and 62 that the D_{20} and D_{19} modes are both related to the M_{20} vibration, and so it is less straightforward to compare between the mono- and disubstituted molecules in these cases.)

This is also an appropriate point to note that the D_{30} vibration also should appear in this region of the spectrum, and the corresponding vibration, M_{30}, has been clearly seen in the spectra of toluene,[5,7] and D_{30} seen for *p*FT (where it is coincident with the $D_{14}D_{20}$ combination band)[13,14] – see Figure 4. However, no such band is present for *p*Xyl, and such a band is also absent in the LIF spectrum of *p*DFB in ref. 47 (where it is denoted Mulliken mode 22). This is explainable in terms of point group symmetry: in a D_{2h} molecule, D_{30} is of b_{2u} symmetry and hence forbidden by both Franck-Condon and Herzberg-Teller (HT) coupling arguments, which cause b_{3g} modes to be allowed; on the other hand, in C_{2v} symmetry, it has b_2 symmetry and so is HT-allowed.

C. Vibrations, Symmetry and Selection Rules

If we assume a complete separation of electronic, vibrational and torsional motion in *p*Xyl, then we expect the $\Delta v = 0$ propensity rule to hold (since the geometries of the S_0, S_1 and D_0^+ states of substituted benzenes are very similar) and, separately, a $\Delta\{m_1, m_2\} = 0$ propensity rule to hold (since the torsional potentials of the three states are expected to be quite similar), where both m_i remain unchanged. We use the notation $\Delta\{m_1, m_2\} = \xi$ ($\xi \neq 0$) to denote a change in either one (but not both) of the m_i quantum numbers; in cases where we wish a

change to refer to the sum of those of both quantum numbers, we shall use $\Delta(m_1 + m_2)$. The most intense bands are hence expected to be associated with transitions that are in line with the torsional and vibrational propensity rules; however, non-totally-symmetric vibrations are also expected via HT coupling. Also, some torsional transitions are seen which do not conform to the $\Delta\{m_1, m_2\} = 0$ propensity rule and these arise from electronic-torsional coupling, as mentioned above in the case of single-rotor molecules. Finally, following on from the discussion given in refs. 8 and 9 for toluene, and refs. 13 and 14 for *p*FT, we may expect to see transitions involving vibration-torsional (vibtor) levels.

1. Transitions involving torsions and the dependence on electronic-torsional coupling

Since the dipole moment, and hence the electric transition dipole moment, will be a function of the two torsional angles, τ_1 and τ_2, its variation can induce torsional activity during an electronic transition, and we shall now examine this. For a single rotor system, it has been argued that the more robust method of examining this is via a Fourier expansion of the dipole moment as a function of the torsional angle – see ref. 39. We outline this in Appendix D, and extend the ideas here to the two-rotor case.

For a two-rotor system the electric dipole transition moment (EDTM) for a pure torsional transition can be written as:

$$\boldsymbol{\mu} = \langle\{m_1{}', m_2{}'\}\,|\langle\psi_1(\boldsymbol{q};\tau_1,\tau_2)|\boldsymbol{\mu}|\psi_0(\boldsymbol{q},\tau_1,\tau_2)\rangle|\{m_1'', m_2''\}\rangle \tag{17}$$

The m_i' represent the internal rotor quantum numbers in the upper electronic state, and m_i'' represent those in the lower electronic state, but remembering that each eigenstate must transform as a definite symmetry species of [3,3]D_{2h} and so involve both rotors; $\boldsymbol{\mu}$ is the electric dipole moment operator; τ_1 and τ_2 are the torsional angles of the two methyl groups and $\boldsymbol{q}$ represents the electronic coordinates. With the defined axis system (see Figure 2), the components of $\boldsymbol{\mu}$ transform as T_a, T_b, and T_c, and hence in G_{72} these symmetries are A_4', $A_1''$and A_2'', respectively – see Table IV. Since the symmetries of the S_1 and S_0 electronic states are A_1'' and A_1', respectively (see Table X for the G_{12} – G_{72} correspondence), the middle

integral will transform as a_4'', a_1' and a_2' for each of $\boldsymbol{\mu}_a$, $\boldsymbol{\mu}_b$ and $\boldsymbol{\mu}_c$, respectively. The next stage is to identify the symmetries of the terms in the Fourier expansion; these will be various combinations of sine and cosine terms of each of $3\tau_i$ and $6\tau_i$. Owing to the propensity rules, we would only expect the $\Delta\{m_1, m_2\} = 0$ or 3 transitions to have appreciable intensity in our spectra, with overall $\Delta(m_1 + m_2) = 6$ transitions expected to be weak, with the latter including cross terms; any higher-order changes are expected to be exceptionally weak.

The dependence of the dipole moment of two-rotor molecules on the torsional angles has been described as a two-dimensional Fourier series.[39,51] We use a complex representation like Eq. (13) for the potential function to expand the dipole moment functions. However, the dipole moment components in general are not totally symmetric functions like the potential function; therefore, the relationships between the coefficients of the series are not identical to those that are valid for the coefficients of the potential function (Eq. (14)). Taking the potential function as an example, the relations between the coefficients need to be modified depending on the symmetry species as follows:

$$V_{j,k} = V_{j,k}(-1)^{j+k+w} = V^*_{-j,-k} = s_1 s_2 V_{-j,-k} = s_1 V_{k,j} = s_2 V_{-k,-j} \tag{18}$$

where $w = (1 - s_3)/2$ and s_1, s_2, and s_3, are the characters of the desired irreducible representation under the operators T, U and D, respectively.

Without going into further details, only the important lowest order terms are listed here for the components of the transition dipole moment. The symmetry species of the transition dipole moment components are obtained as the direct product of the species of T_q (q = a, b or c) and of the species of the electronic wavefunctions of the S_0 and S_1 states.

$$a_4'' : \boldsymbol{\mu}^a(\tau_1, \tau_2) = C_3^{-C}(\cos 3\tau_1 - \cos 3\tau_2)$$

$$a_1' : \boldsymbol{\mu}^b(\tau_1, \tau_2) = C_0 + C_{33}^c \cos 3\tau_1 \cos 3\tau_2 + C_{33}^s \sin 3\tau_1 \sin 3\tau_2$$

$$a_2'\colon \boldsymbol{\mu}^{c}(\tau_1,\ \tau_2) = C_{33}^{-SC}(\sin 3\tau_1 \cos 3\tau_2 - \cos 3\tau_1 \sin 3\tau_2) \qquad (19)$$

where the subscripts on the coefficients are analogous to those of the single rotor case, and the superscripts denote the cosine/sine nature of the terms, in an obvious fashion. We expect $\Delta\{m_1,m_2\} = 0$ transitions to be *b*-type and the most intense, followed by the *a*-type $\Delta(m_1,m_2) = 3$ ones, which can gain intensity via electronic-torsion (Herzberg-Teller) intensity stealing (see below). Transitions that have $\Delta(m_1+m_2) = 6$ (*b*-type and *c*-type) are expected to be weak and any higher-order transitions, are expected to be very weak.

Earlier, we noted that we would expect the four lowest internal rotor levels, {0,0}, {0,1}, {1,1} and {1,-1} (hereafter referred to as the "cold" levels) still to be populated in the S_0 state after free jet expansion (since they are each associated with different symmetry nuclear spin functions), and consequently transitions can occur out of any of these. We now consider which internal rotor levels are expected to be accessed via direct or electronic-torsion-induced excitation from these four "cold" levels; we indicate in bold those transitions that are expected to have significant intensity.

For $\{m_1'',m_2''\} = \{0,0\}$, the symmetry is a_1', and so the states with lowest allowed values of m' that give an overall totally symmetric EDTM are:

a-type: **$\{0,3\}^{--}$ = $\{0,3(+)\}^{-}$**

b-type: **{0,0}**, $\{3,3\}^{+}$, $\{3,-3\}^{+}$, $\{0,6\}^{++} = \{0,6(+)\}^{+}$

c-type: $\{3,-3\}^{-}$, $\{0,6\}^{-+} = \{0,6(-)\}^{-}$

For $\{m_1'',m_2''\} = \{0,1\}$, the symmetry is g'' and so possible values of m' that give an overall totally symmetric EDTM) must have symmetries g' and g'', and are (recalling that the notation includes other signed values of m_{i-} see Table V):

a-type: **{0,2}, {-3,1}, {3,1}, {0,4}**, {3,-5} and {-3,-5}

b-type: **{0,1},** {3,-2}, {-3,-2}, {-3,4}, {0,5}, {3,4}

c-type: **{0,1}**, {3,-2}, {-3,-2}, {-3,4}, {0,5}, {3,4}

For $\{m_1'',m_2''\}$ = {1,1}, the symmetry is e_3' and so possible values of m' that give an overall totally symmetric EDTM must have symmetries e_4'', e_3' and e_4' and are:

a-type: **{1,-2}$^-$, {1,4}$^-$**, {-2,-5}$^-$

b-type: **{1,1}**, {-2,-2}, {4,-2}$^+$, {1,-5}$^+$, {4,4}

c-type: {4,-2}$^-$, {1,-5}$^-$

For $\{m_1'',m_2''\}$ = {1,-1}, the symmetry is e_1' and so the possible values of m' (that give an overall totally symmetric EDTM) are:

a-type: **{1,2}$^-$, {1,-4}$^-$**, {-5,2}$^-$

b-type: **{1,-1}**, {2,-2}, {4,2}$^+$, {1,5}$^+$, {4,-4}

c-type: **{1,-1}**, {2,-2}, {4,2}$^+$, {1,5}$^+$, {4,-4}

Thus, we expect to see transitions involving the bolded levels above as the most distinct in our REMPI spectra. Other transitions might be observed as the result of (a generalized form of) Fermi resonance; the latter would also lead to perturbed band positions. When recording ZEKE spectra, we would, of course, be selecting a particular S_1 level, and so this will determine what ZEKE bands are expected, with the $\Delta v = 0$, $\Delta(m_1+m_2) = 0$ bands expected to be the most intense, and $\Delta(m_1+m_2) = 3$ bands also being expected; bands with changes in vibration quantum number may also be observed depending on the geometry change during the $D_0^+ \leftarrow S_1$ transition.

2. Torsional transitions and Herzberg-Teller coupling

As is well known, in substituted benzene molecules, "symmetry or Franck-Condon forbidden" vibrations can appear and, in molecules such as toluene and *p*FT, also "forbidden" torsions may be observed. These arise as a result of intensity stealing via Herzberg-Teller (vibronic) coupling, and its analogue for torsions, in a similar manner to the well-known case of benzene. Employing point group symmetry, the relevant state in benzene is the $\tilde{C}^1E_{1u}$ state, with e_{2g}

vibrations mediating the vibronic coupling for the $\tilde{A}\,^1B_{2u}$ state; in D_{2h} the relevant state is the $\tilde{B}^1B_{1u}$ state, with b_{3g} vibrations mediating intensity stealing from a higher $^1A_{1g}$ state, which is derived from the benzene $\tilde{C}$ state. As mentioned above, in the cases of toluene and *p*FT, there has been shown to be an analogous electronic-torsion intensity stealing mechanism, and this leads to the 3(+) torsion being active in the $S_1 \leftarrow S_0$ transition, arising from a $m' \leftarrow m''$ transition of 3(+) ← 0. Using MSG symmetry, the a_1'' vibrations and torsions of the S_1 ($^1A_1''$) state gain intensity via intensity stealing from a higher $^1A_1'$ state, again which is derived from the benzene $\tilde{C}$ state. More generally, $\Delta m = 3$ transitions gain intensity via this mechanism and hence it is also possible to see 4 ← 1 and 2 ← 1 transitions (again, recalling that the *m* are signed). Also, possible to see but much more weakly, are $\Delta m = 6$ transitions and even weaker still for higher changes of $\Delta m = 3n$ (n = integer).

In the case of *p*Xyl, similar considerations hold. First we note that in [3,3]D_{2h} the $S_1 \leftarrow S_0$ transition can be denoted $\tilde{A}\,^1A_1'' \leftarrow \tilde{X}^1A_1'$, and the relevant excited electronic state to which electronic-torsion coupling needs to occur when exciting from {0,0} has A_4' symmetry (again this will be derived from the benzene $\tilde{C}$ state); thus, we expect a_4'' symmetry torsions to be active via this mechanism, which Table IV reveals to be $\{0,3\}^{--}$, which (see Section II.B.5 and Appendix C) may be written as $\{0, 3(+)\}^-$. In a similar way, exciting from {0,1}, which has g'' symmetry, requires g' torsions, and so we expect {0,2}, {-3,1}, {3,1} and {0,4} amongst others, to be active; exciting via {1,1}, which has e_3' symmetry, requires e_4'' torsions, and so we expect $\{1,-2\}^-$ and $\{1,4\}^-$ to be active; and finally, exciting via {1,-1}, which has e_1' symmetry, requires e_2'' torsions and hence we expect $\{1,2\}^-$, $\{1,-4\}^-$ to be active. Note that we have only considered $\Delta(m_1+m_2) = \pm 3$ transitions, as these are expected to be the most intense.

3. Vibration-torsion (vibtor) states

Finally, we note that vibtor levels have been seen in toluene and *p*FT and it is expected that such levels will be seen for *p*Xyl. For a vibtor level to be FC-active when exciting from the {0,0} torsional level, we expect the direct product of the vibrational symmetry and the torsional symmetry to be totally symmetric, A_1', for *p*Xyl; however, there will also be transitions from the other still-populated torsional levels, and these will need to be considered when assigning the spectrum. First, we need to determine what the equivalent of the D_{2h} symmetries are in G_{72}; the correspondence between these, using the axis systems shown in Figures 1 and 2, are

given in Table X. Then, in Table XI we tabulate the symmetries of the vibtor levels that arise when each of the torsional levels interact with each of the three lowest energy vibrations, D_{20}, D_{19} and D_{14}. As may be seen, as well as bands from the "pure" {0,0} (intense) and $\{0,6(+)\}^+$ (weak) torsions when exciting from {0,0} in the S_0 state, we may also expect to see symmetry-allowed transitions to D_{20} $\{0,3(-)\}^-$, D_{19} $\{0,3(-)\}^+$ and D_{14} $\{0, 6(-)\}^+$ for the $S_1 \leftarrow S_0$ excitation. The fact that two different {0, 3(-)} levels are associated with the D_{20} and D_{19} vibrations in the FC-allowed vibtor levels arises as a result of the different symmetries of these vibrations under D_{2h} (and hence G_{72}); in *p*FT both D_{20} m = 3(-) and D_{19} m = 3(-) levels were seen with reasonable intensity, with both of these vibrations interacting with the same torsional level under the lower-order MSG. Additionally, there will also be corresponding transitions from the {0,1}, {1,1} and {1,-1} levels, which will access different upper vibtor levels in each case and these will be discussed at appropriate points below.

It will also be the case that vibtor levels of the same symmetry can interact with each other and with "pure" torsional levels that have the corresponding symmetry. As has been shown for toluene[8,9] and *p*FT,[13,14,15] these interactions can shift levels in wavenumber and hence cause transitions not to be in the expected position. We shall comment on this below for some of the transitions observed, but will not report a full analysis of this in the present paper. We expect vibtor transitions involving the same vibrational change, but different "cold" torsional levels to be at relatively similar transitions energies; however, these will be at different energies owing to the different upper levels accessed and perhaps also as a result of different symmetry levels interacting differently with other vibtor levels. The latter suggests that we may observe splitting of bands, if this effect is sizeable.

In Figure 4 we show expanded views of the pertinent region of the low-wavenumber regions of the REMPI spectra of toluene, *p*FT and *p*Xyl. It is striking that the region below 100 cm^{-1} is very similar in all three spectra, but even more striking is the very similar appearance of the spectra of *p*FT and *p*Xyl below 200 cm^{-1}. The assignments of the toluene spectrum come from refs. 9 and 39 and those for *p*FT come from refs. 13, 14 and 15. The assignments for *p*Xyl are from the present work and will be discussed in more detail below. For now, we note that the assignments for *p*Xyl are very similar to *p*FT, in that the same values of the m quantum numbers are associated with bands at similar wavenumbers; however, because of the different (higher) symmetry of *p*Xyl arising from the two methyl groups, the levels are not the

same and loosely consist of various symmetric and asymmetric combinations of the corresponding single-rotor levels.

In the subsections below, we shall deal with each REMPI band in turn, discussing its assignment in terms of the allowed symmetries of the S_1 internal rotor levels that can be accessed from the cold $\{m_1, m_2\}$ levels (see Appendix B). Thus, we need to consider population of S_1 internal rotor levels when exciting from each of the {0,0}, {0,1}, {1,1} and {1,-1} levels taking into account the symmetries of the components of the transition dipole moment (see Section IV.C.1). In all cases, it transpires that more than one S_1 internal rotor level will be populated. We will treat various REMPI bands together and, in each case, show the relevant section of the REMPI spectrum, together with ZEKE spectra that have been recorded. In a number of cases, ZEKE spectra are recorded at wavenumbers corresponding to different parts of a REMPI feature to establish if there are distinct overlapping contributions.

We first note that excitations involving totally-symmetric vibrational levels will consist of four associated internal rotor transitions in each case, i.e. the $\Delta\{m_1, m_2\} = 0$ transitions from the four "cold" internal rotor levels just noted; these will all appear almost completely overlapped in our spectra as the transition energies are all expected to be within 1 cm^{-1} of each other. We shall also see that various non-totally symmetric vibrations will be seen via HT coupling and vibtor transitions will be seen, again involving non-totally-symmetric vibrations.

(a) Excitation via {0,0}, {0,1}, {1,1}, {1,-1}

In Figure 5(a) we show an expanded view of the pertinent region of the REMPI spectrum where the "pure" torsional excitations are located. We indicate the bands whose wavenumbers correspond to the excitation positions we employed to record ZEKE spectra. In Figure 5(b) we show the ZEKE spectrum when exciting via the origin transition focusing on the torsional region. Being a transition involving the totally-symmetric zero-point vibrational energy levels, the most intense REMPI feature will consist of the four overlapped bands associated with the four "cold" torsional levels and as a consequence, the ZEKE spectrum will also consist of transitions from these four levels into various levels of the cation; the most intense will be the four $\Delta\{m_1, m_2\} = 0$ transitions which will appear as a single overlapped ZEKE feature as the torsional potentials in the S_1 and D_0^+ states are expected to be very similar. The wavenumber of this band defines the adiabatic ionization energy (see ref. 21).

(b) Excitation via {0,2}, {1,2}$^-$ and {1,-2}$^-$

We recorded a ZEKE spectrum via the REMPI band at 0^0 + 16 cm^{-1} and this is shown in Figure 5(c). It may be seen to consist of a main band at 15 cm^{-1}, with a shoulder corresponding to the origin position. The REMPI band is expected to consist of three overlapped transitions: {0,2} ← {0,1}, {1,-2}$^-$ ← {1,1} and {1,2}$^-$ ← {1,-1} and hence each of the S_1 levels could be the starting level for a ZEKE transition. We expect the $\Delta\{m_1, m_2\} = 0$ transitions to be the most intense, but we may also see other transitions induced by electronic-torsional coupling. By considering the symmetry of each of these, plus the symmetry of the dipole moment integral we find that the {0,1} ← {0,2} and {1,1} ← {1,-2}$^-$ transitions can be induced via electronic-torsional coupling and hence these could both be contributing to the weak ZEKE band at the origin. There are also some very weak bands to higher wavenumber, which could arise from transitions to other levels, induced by electronic-torsional coupling.

(c) Excitation via {0, 3(-)}$^-$ and {0, 3(+)}$^-$

We then consider the ZEKE spectra when exciting through the m = 3 levels, which are shown in Figures 5(d) and 5(e). The question arises as to which {0,3} levels could be accessed in the S_1 state, as there are four such of these. First, we note that in *p*FT[13], consistent with toluene,[39] it has been concluded that the more intense band was associated with the 3(+) level and arose as a result of a transition from $m'' = 0$ via electronic-torsional coupling in the S_1 state, similar to that in toluene[39,40] and as summarized above. For *p*Xyl the S_1 $^1A_1''$ state in G_{72}, and so the expected torsional level that arises from corresponding coupling when exciting from the {0,0} S_0 level is {0,3}$^{--}$, which can be written as {0,3(+)}$^-$, as noted above (see also Appendix C).

A lower wavenumber, and significantly less intense, band in the REMPI and 2D-LIF spectra of toluene have been seen and assigned as arising from the 3(-) state,[5,7,8,19,39,40] attributed to torsional-rotational coupling.[39,40] We noted that this band in the spectrum of *p*FT had the same symmetry as the cation, which is $^2A_2''$ for *p*Xyl, since the corresponding band for the cation was seen in the ZEKE spectrum recorded via the origin and arose via electronic-torsional coupling with the first excited cation electronic state.[13] If the same mechanisms hold here for *p*Xyl, then the expected level is {0,3}$^{-+}$ = {0,3(-)}$^-$ and could be contributing to the REMPI band at 40 cm^{-1}. Although weak, the ZEKE spectrum recorded via the 40 cm^{-1} band, Figure 5(d), consists of what looks like a single $\Delta\{m_1,m_2\} = 0$ band, with any other features

being too weak to see. On the other hand, exciting from the {0,1} level in the S_0 state would allow the {3,1} and {-3,1} levels to be accessed and so transitions to these could be contributing to the REMPI feature. Further, these transitions can steal intensity via a generalized form of HT coupling, and so perhaps are likely to be the main contributors to this feature. Contributions from the {1,-1} level in the S_0 state are also possible, but would give rise to features that will be coincident with those from the {1,1} state, within our resolution.

The spectrum obtained when exciting through the $\{0,3(+)\}^-$ level at 53 cm^{-1}, Figure 5(e), again appears to consist of an intense feature assumed to be the $\Delta\{m_1, m_2\} = 0$ transition, but with a weak $\Delta\{m_1, m_2\} = -3$ feature visible for the origin. Further, since the two features are clearly distinct in the S_1 state for *p*Xyl, this suggests a clear assignment of two ZEKE bands, and places the $\{0,3(-)\}^-$ band *below* the $\{0,3(+)\}^-$ band in the cation. This assignment order is consistent with that of the $m = 3$ levels in *p*FT presented in ref. 16 and also in our recent conclusions for *p*FT.[13] Additionally, this conclusion suggests that the assignment of the $m = 3$ region of the toluene ZEKE spectrum by Lu et al.[19] is incorrect, with the band profile therein being affected by a rotational envelope effect – see reference 13 for a more-detailed discussion.

Earlier (Section II.B.6) we discussed the main torsional potential terms that are expected for *p*Xyl and showed the interaction matrix for the four {0,3} functions. The eigenfunctions in G_{72} are found by diagonalizing this and Table IX shows the resultant eigenfunctions (see also Table V and Section II.B.6) and energies, where E_{03} is the free internal rotor energy. Looking at the REMPI spectra in Figure 4(c) and noting the discussion above, then we see that there is a good correspondence between the positions of the $m = 3(+)$ bands in toluene and *p*FT and the corresponding $\{0,3(+)\}^-$band in *p*Xyl. If the 40 cm^{-1} band were solely arising from transitions to and $\{0,3(-)\}^-$ from the {0,0} level, then the fact that it is in almost the same position as the 3(-) band in toluene would suggest that the interactions are similar. This is surprising as the interactions in toluene involve the M_{20} vibration, which is higher in wavenumber than the D_{20} vibration in *p*Xyl that would be involved here. Assigning this band solely to the {3,1} and {-3, 1} levels does not help as the D_{20} {0,1} level could be interacting and so affecting the position. Currently, we note this correspondence in the position of the $m_2 = 3$ bands in *p*Xyl with those in toluene and *p*FT is interesting and seems to arise from coincidences in the overall magnitudes of the interactions in the various molecules.

From the results in Table IX, we can see that the $V_{6,0}$ term plays the equivalent role of V_6 in single-rotor systems and splits the pair of $\{0,3(+)\}^+$ and $\{0,3(+)\}^-$ states from the $\{0,3(-)\}^+$ and $\{0,3(-)\}^-$ pair; while within each pair, the ($V_{3,3}\pm V_{3,-3}$) term will cause a splitting between the pairs of $\{0,3(+)\}^\pm$ and $\{0,3(-)\}^\pm$ states. The indications from the spectra, comparing the < 200 cm^{-1} regions of *p*FT and *p*Xyl, is that the $V_{6,0}$ term is the largest, and the ($V_{3,3}\pm V_{3,-3}$) terms are relatively small. Further, if the 40 cm^{-1} REMPI band contains contributions from the $\{0,3(-)\}^-$ level, then this lies below the $\{0,3(+)\}^-$ one; then the expectation is that the $V_{6,0}$ term is negative with the present axis system and definition of the torsional angle. Of course, caution is required since the 40 cm^{-1} band may contain more than one contribution and also we know that vibration-torsion interactions are likely to be present, and this will affect spectral positions. If the relative energies of enough levels are measured, however, a more accurate picture of the energy levels should be possible via a full vibration-torsional perturbation analysis.[8,9,15]

(d) Excitation via {0,4}, $\{1,4\}^-$ and $\{1,-4\}^-$

Between 68 and 82 cm^{-1} there is a broad REMPI band that appears to consist of at least two features. This wavenumber region is expected for the location of bands associated with transitions involving $m_i = 4$ on one of the rotors. The symmetry of the TDM suggests that three transitions could be contributing to this feature: $\{0,4\} \leftarrow \{0,1\}$, $\{1,4\}^- \leftarrow \{1,1\}$ and $\{1,-4\}^- \leftarrow \{1,-1\}$. Given the band profile, we recorded spectra at three different wavenumbers in the profile corresponding to 0^0 + 72 cm^{-1}, 0^0 + 76 cm^{-1} and 0^0 + 79 cm^{-1}; these three spectra are shown in Figure 6. Some caution is required in interpreting spectra recorded within a single REMPI band as the sampling of different tranches of the rotational profile can lead to differently shaped ZEKE bands.[13]

In the present case we can see that exciting at 72 cm^{-1} gives rise to a main ZEKE band at 77 cm^{-1}, together with a weak band at the origin and another weak band at 104 cm^{-1}; exciting at 76 cm^{-1} gives rise to a band that appears to show a double maximum at 77 and 80 cm^{-1}, together with weak bands at 103 cm^{-1} and the origin; finally, when exciting at 79 cm^{-1}, the band at 77 cm^{-1} may be seen, together with a possible shoulder at 86 cm^{-1}. Thus, with the

caveat above regarding rotational profiles, there are indications that the REMPI feature may have more than one contribution.

The weak band at the origin arises from the {0,1} ← {0,4} and {1,1} ← {1,4}$^-$ transitions, while the strong band arises from $\Delta\{m_1, m_2\} = 0$ transitions involving all three populated S_1 torsional levels. Although electronic-torsional coupling can lead to levels with $m_i = 5$ being accessed, the band at 105 cm^{-1} seems too low in wavenumber for this. Based on our experience with *p*FT and spectra to be discussed below, we expect to see bands associated with the D_{20} band. Indeed the D_{20} {0,1} level has the correct symmetry to interact with the {0,4} level (both are *g*′ symmetry) and this is also consistent with the wavenumber expected for the D_{20} vibration (on the basis of quantum chemical calculations presented in ref. 21, and other spectra presented later). Additionally, a second contribution to this band is possible from interaction of the D_{20} {1,1} level with the {1,4}$^-$ level (both are e_4″ symmetry). It is difficult, based on the available spectra, to disentangle the effect of rotational envelope changes and differing contributions to the different bands/band profiles, observed when exciting through the features in the REMPI spectrum at 68–82 cm^{-1}. Interaction with the different D_{20} torsional levels would give a further mechanism for such band profile changes and/or splitting from differing interactions between the (pairs of) different symmetry levels. We can say that interactions between the states mentioned above would tend to lead to the {0,4} and {1,4}$^-$ levels moving down in wavenumber, but the {1,-4}$^-$ level remaining in position – this then provides a possible mechanism for the broadening/splitting that is seen in the 68–82 cm^{-1} feature.

4. Excitation at wavenumbers 100-120 cm^{-1}

We now move on to the REMPI feature at ~ 110–120 cm^{-1}, see Figure 7(a), which is relatively broad and so may consist of more than one band. Its wavenumber suggests possible contributions from $m_i = 0$, 1 levels associated with D_{20} as well as levels that have $m_1 = 0$, 1 and $m_2 = 5$. We have recorded ZEKE spectra at three positions, A, B and C as marked in Figure 7(a) and these spectra are shown in Figures 7(b)–(d). The indications from these spectra are that there are three contributions to the REMPI band, with the low wavenumber edge (A) giving rise to a ZEKE band at ~ 102 cm^{-1}, the centre of the band (B) giving rise to the ZEKE band at 113 cm^{-1} and the high-wavenumber side (C) giving rise to the ZEKE band at 122 cm^{-1}.

First, we note that we did not see any significant variation of the REMPI feature with backing pressure and so rule out a contribution from any hot bands. When exciting at position A (at ~108 cm^{-1}), the spectrum in Figure 7(b) shows what looks like two clear, but overlapping bands, one at 102 cm^{-1}, which we assume is the same band seen when exciting via the m_i = 4 levels (see Figure 6), i.e. accessing D_{20} {0,1} in the cation, and a more intense band at 111 cm^{-1}. Essentially the same two ZEKE features, but with intensity changes, are observed when exciting at position B (at ~110 cm^{-1}); however, when exciting at position C (at 114 cm^{-1}), a very different spectrum is seen, Figure 7(d), with a single ZEKE band at 122 cm^{-1}. Very similar behaviour was observed for *p*FT[13] and so we expect an assignment in line with this where *m* = 5 levels were accessed, as well as vibtor levels involving D_{20}. First, we note that when exciting from the various cold {m_1, m_2} levels, symmetry dictates that we can access the {0,5}, $\{1,-5\}^-$, $\{1,-5\}^+$ and $\{1,5\}^+$ S_1 levels, which are all expected at transition wavenumbers that will be essentially coincident at our resolution. These have symmetries of g'', e_4', e_3' and e_1', respectively, and each of these has the same symmetry as D_{20} {0,2}, D_{20} $\{1,-2\}^+$, D_{20} $\{1,-2\}^-$ and D_{20} $\{1,2\}^+$, respectively. The latter are all expected at about the same unperturbed transition wavenumber and at approximately the same separation from the respective m_2 = 5 levels, from which they are all related by a Δv = 1, $\Delta\{m_1, m_2\}$ = 3 change; hence, although there may be small differences in the coupling terms, we may reasonably expect a fairly similar interaction between the respective pairs of states and hence resulting eigenfunctions that have approximately the same transition wavenumbers and separations.

To summarize, the ZEKE band at 102 cm^{-1} is associated with the D_{20} {0,1}…{0,4} eigenstate, which is of g' symmetry with a dominant contribution at position A, and this eigenstate does not interact with the other levels within the REMPI feature. At position B, there is a small contribution from the high-wavenumber edge of the D_{20} {0,1}…{0,4} eigenstate, but the major contribution is from eigenstates arising from transitions involving the D_{20} {0,2}…{0,5}, D_{20} $\{1,-2\}^+$…$\{1,-5\}^-$, D_{20} $\{1,-2\}^-$…$\{1,-5\}^+$ and D_{20} $\{1,2\}^+$…$\{1,5\}^+$ eigenstates, which lead to the 111 cm^{-1} band. At position C (114 cm^{-1}), we expect the "partner" eigenfunction contributions: {0,5}…D_{20} {0,2}, $\{1,-5\}^-$…D_{20} $\{1,-2\}^+$, $\{1,-5\}^+$…D_{20} $\{1,-2\}^-$ and $\{1,5\}^+$…D_{20} $\{1,2\}^+$.

Given the above interactions, it is initially surprising that both the 111 cm^{-1} and 122 cm^{-1} ZEKE bands do not appear in each spectrum when exciting at both positions B and C; however, this

may be rationalized if both the torsional potential and D_{20} vibrational wavenumber in the S_1 and D_0^+ states are very similar. Under such a scenario the interactions between the pertinent levels in both electronic states would be very similar and hence transitions would be largely "diagonal" – i.e. between the same eigenstates with almost the same make-up in each state.

5. Comparison with previous work

As mentioned above, Breen et al.[23] reported a REMPI spectrum of *p*Xyl in the range 0–110 cm^{-1}. Assignments of the bands were given in terms of excitations of independent torsions of the two methyl groups, with some involving two $\Delta m_i = 3$ changes, one on each rotor, i.e. $\Delta(m_1 + m_2) = 6$; as we have noted above, we anticipate such transitions to be extremely weak. Further, inspection of Figure 4 shows that essentially the same features are seen in the spectra of *p*FT (a single-rotor system) and *p*Xyl (a two-rotor system); and, in the range 0–85 cm^{-1}, essentially the same features are seen in the REMPI spectra of these two molecules and toluene. We therefore conclude that assignments in ref. 23 that involve more than one $\Delta m = 3$ transition in *p*Xyl are likely incorrect, and we have reassigned those here.

We are in general agreement with the assignment of the origin, but which we assign to the four essentially coincident $\Delta\{m_1,m_2\} = 0$ transitions involving {0,0}, {1,0}, {1,1} and {1,-1}. In ref. 23, this was assigned to three of the same transitions, albeit referring to two (essentially degenerate) transitions involving the (1,0) and (0,1) methyl-localized states. Related comments apply to their assignment of pairs of m_1^2 and m_1^4 transitions, which we assign to three coincident transitions in each case. We loosely concur with their assignment of the $m_0^{3(+)}$ transition, which we designate as a transition to $\{0,3(+)\}^-$. It is peculiar that they noted a weak band at 40.5 cm^{-1} in their spectrum in Figure 6 of their work, while also calculating the position of the $m = 3(-)$ state at 41 cm^{-1}, but did not assign that weak band, which we attribute here to transitions that have one $m_i = 3$ level. Two bands whose assignment we do not agree with are those of the feature at 72 cm^{-1}, assigned as [2, 3(+)] ← (1,0) in ref. 23, or the one at 110 cm^{-1}, assigned as [3(+), 3(+)] ← (0, 0) therein. In the case of the 72 cm^{-1} band the assignment of ref. 23 involves a $\Delta(m_1 + m_2) = 6$ transition, and hence we would expect this to be extremely weak; we have discussed the assignment of this feature via ZEKE spectra recorded at three different wavenumbers. In the case of the 110 cm^{-1} band: again, we first note that the assignment of ref. 23 involves a $\Delta(m_1 + m_2) = 6$ transition and hence would be

expected to be very weak; secondly, we see a corresponding feature in the single-rotor *p*FT spectrum at essentially the same position; and thirdly, we would expect a ZEKE band at ~ 94 cm^{-1} when exciting at the corresponding wavenumber, if the assignment of ref. 23 were correct, while in actuality, the main bands are at 113 cm^{-1} and 121 cm^{-1}. In summary, our assignments are based on a more complete consideration of the molecular symmetry of the system; the expected intensities of the transitions in terms of $\Delta(m_1+m_2)$ changes; the observation of corresponding features in the single-rotor *p*FT and two-rotor *p*Xyl cases; and the observed ZEKE bands. As a consequence, we feel the present assignments are more reliable.

The only other previous work that has addressed the assignment of the "pure" torsional transitions for *p*Xyl upon photoionization is the MATI study of Held et al.,[31] who only recorded a spectrum via the origin. We essentially agree with their assignment of the origin band as a composite of transitions involving m_i = 0,1 levels of the two rotors (see comments above), but our discussion is more complete in molecular symmetry terms and we conclude there are four such transitions. We also essentially agree with the assignments of the band at ~ 15 cm^{-1} in terms of transitions between cold {m_1, m_2} levels in S_0 involving m_i = 0 and 1, to S_1 levels involving m_i = 2, but again we take full account of molecular symmetry. We disagree with the assignment of the ~43 cm^{-1} band as involving the m = 3(+) levels, as discussed above, where we have assigned this to a transition to the {0, 3(-)}$^-$ level. We also disagree with the assignment of the ~112 cm^{-1} band, which Held et al.[31] assign to a hot-band transition involving an m_i = 2 level in the S_1 state, while we have noted above that we assign this to various transitions involving cold S_0 levels and S_1 m_i = 5 and vibtor levels of D_{20}.

6. Excitation via other vibtor levels involving D_{20}

In Figure 8(a) we indicate the REMPI transitions that involve the various other vibtor levels of the D_{20} vibration. In Figure 8(b)–(f), we show the ZEKE spectra obtained when exciting through these various intermediate levels. The deduction that these correspond to vibtor levels involving the D_{20} vibration is consistent with the calculated vibrational wavenumbers, and also consistent with expectations based on toluene[9] and *p*FT.[13,14]

For an overall totally-symmetric vibtor level, we require the D_{20} vibration to combine with a torsion of a_2'' symmetry, and so wavenumber considerations lead to this being $\{0,3(-)\}^-$ – see Table XI. Hence, when exciting from the S_0 {0,0} level, we can access the D_{20} $\{0,3(-)\}^-$ level on symmetry grounds (via a generalized form of the Franck-Condon principle). However, we should also consider transitions from the other cold {m_1, m_2} levels and looking at the symmetries of the four such levels with m_1 = 0 or 1 and m_2 having a value of 3 (or equivalent), we see that the S_1 D_{20} {3,1} and D_{20} {-3, 1} levels are accessible from the S_0 {0,1} level. The REMPI band at 135 cm^{-1} is then assigned to these two transitions. As a consequence, we expect the intense feature at 146 cm^{-1} in the ZEKE spectrum in Figure 8(b) to be three overlapped $\Delta(v,m)$ = 0 bands, and so correspond to transitions to D_{20} $\{0,3(-)\}^-$, D_{20} {3,1} and D_{20} {-3,1}. We use $\Delta(v,m)$ = 0 to represent a combination of the Δv = 0 and $\Delta\{m_1, m_2\}$ = 0 transitions. Close inspection of this REMPI feature reveals that it has the appearance of a double band, and so we recorded spectra at excitation wavenumbers corresponding to the two maxima, at 0_0^0 +135 cm^{-1} and 0_0^0 +138 cm^{-1}.

When exciting at 135 cm^{-1}, a rich ZEKE spectrum is seen with the intense $\Delta(v,m)$ = 0 band at 146 cm^{-1}, which is assigned to the cation D_{20} $\{0, 3(-)\}^-$ band; to higher wavenumber is the expected $D_{11}D_{20}$ $\{0,3(-)\}^-$ combination band – combinations of the main $\Delta(v,m)$ = 0 band with the D_{11} vibration are seen in the ZEKE spectra of many substituted benzenes. Also common in the case of *p*FT,[12,13] were combination bands with the non-totally-symmetric vibrations D_{19} and D_{14}; here we see the latter at 487 cm^{-1}, but do not discern the former, likely owing to the signal-to-noise. Another common observation in *p*FT[13] was the observation of Δv = -1 and Δm = -3 bands; corresponding bands are indeed seen here at 46 cm^{-1} from overlapped transitions to $\{0\ 3(-)\}^-$, {3,1} and {-3,1} and to D_{20} {0,0} and D_{20} {0,1} at 97 cm^{-1}. Transitions to other totally-symmetric bands appear at: 204 cm^{-1} – assigned to a transition to $2D_{20}$ – see below; 617 cm^{-1} – assigned as a transition to $2D_{19}D_{20}$ $\{0,3(-)\}^-$; and 188 cm^{-1}, tentatively assigned as a transition to $\{0, 6(+)\}^+$. A band is observed at 288 cm^{-1} which currently remains unassigned, but may be due to a state that has arisen from an interaction that gives it unexpected intensity in a perturbed position.

When exciting at 0^0 + 138 cm^{-1} we see a weaker spectrum, but the two most intense bands appear at almost the same wavenumber as in the spectrum exciting at 0^0 + 135 cm^{-1}. Other,

weaker bands are essentially absent although there is a band at 204 cm^{-1}, which can be associated with $2D_{20}$. Thus, there is no conclusive evidence that the 135 and 138 cm^{-1} REMPI bands are associated with different S_1 levels, but we note that in this region we can expect transitions from the "cold" S_0 torsional levels to levels involving D_{20} and levels with m_i = 3. Hence, as well as the D_{20} {0, 3(-)}$^-$ level, we may also expect to see the D_{20} {3,1} and D_{20} {-3,1} levels accessed from S_0 {0,1}, which will have *g*″ symmetry (Table XI). In the absence of any interactions between other levels, these three transitions will be expected at almost an identical wavenumber, but since they have different symmetry, then this could be an explanation for the observed splitting of the band. The most obvious cause of this would be an analogue of an interaction seen in toluene and *p*FT, where the *m* = 6(+) level interacted with the D_{20} *m* = 3(-) level, with possible involvement for *p*FT from the $2D_{20}$ level, all of which were totally-symmetric levels. There is also the possibility that vibtor levels involving D_{19} could be involved in other cases (see below). In the case of *p*Xyl interactions, the corresponding interactions would be between D_{20} {0,3(-)}$^-$, {0,6(+)}$^+$ and $2D_{20}$, specifically $2D_{20}$ {0,0}. That these may be interacting could be supported by the observation of both a band at ~ 188 cm^{-1}, which could be attributable to {0,6(+)}$^+$ and a band a 204 cm^{-1}, which seems likely to be $2D_{20}$ {0,0}. Given the position of the D_{20} ZEKE band mentioned above, it does seem that the overtone level is at a lower wavenumber than might be expected. Further, comparison between the spectra of *p*FT and *p*Xyl indicates that although the D_{20} {0,3(-)}$^-$ level, and (see below) vibtor level(s) involving D_{20} and m_i = 4, are in almost identical positions for the two molecules, the $2D_{20}$ band has moved to lower wavenumber. Given that the levels to lower wavenumber all appear in approximately the same position – indicting very similar non-perturbed and perturbed positions and, hence, very similar overall interactions – then the suggestion is that the $2D_{20}$ level has been pushed down in wavenumber via interaction with a higher-wavenumber level, with the D_{19} {0,3(-)}$^+$ level appearing to be the most likely. We note that all of the D_{19} vibtor levels in *p*Xyl are to lower wavenumber than those in *p*FT, in line with the expected lowering in the D_{19} wavenumber between the two molecules (see calculated vibrational wavenumbers in ref. 21). Thus, interactions between $2D_{20}$ {0,0} and D_{19} {0,3(-)}$^+$ will be more significant in *p*Xyl than the corresponding interaction in *p*FT. If this is the cause of the splitting, then for this to lead to the split features at 135 and 138 cm^{-1}, it suggests a stronger interaction between the a_1′ levels relative to the *g*″ ones.

This assignment disagrees with that of Held et al.,[31] who assigned the ZEKE band (only a single band was mentioned) at ~146 cm^{-1} to a transition commencing at m = 3(+) level, which was thought to be accessed via a hot band transition; however, it seems unlikely in a jet-cooled experiment that excitation of any levels involving m = 3(+) in the S_0 state will be observed, and so this assignment cannot be correct. The same band (at 144 cm^{-1}) was reported by Gunzer and Grotemeyer[29] using MATI spectroscopy and assigned as an unspecified methyl torsion transition; again, an assignment with which we do not concur. Blease et al.[24] saw a band in their REMPI spectra at 136 cm^{-1} but this was unassigned.

There is a weak REMPI band at 153 cm^{-1} and excitation through this band yields a single $\Delta(v,m)$ = 0 ZEKE band at 156 cm^{-1} – see Figure 8(d). Our best assignment for the REMPI band is to a vibtor level involving D_{20} and a level with m_i = 3, with a transition to the D_{20} $\{0,3(+)\}^+$ being allowed via a generalized form of Herzberg coupling, being of a_2' symmetry. The assignment of the REMPI band to a transition to D_{20} $\{0,3(+)\}^+$ is consistent with a very weak D_{20} m = 3(+) feature seen in the 2D-LIF spectrum of *p*FT.[14]

To slightly higher energy in the REMPI spectrum is a band at 173 cm^{-1} that can be assigned as the D_{20} $\{0,4\} \leftarrow \{0,1\}$ transition; again, ionization through this level, see Figure 8(e), leads to the expected $\Delta(v,m)$ = 0 band in the ZEKE spectrum in a position (176 cm^{-1}) that leads to straightforward assignment to the corresponding cation D_{20} m={0,4} vibtor level. In addition, to higher wavenumber (618 cm^{-1}) we observe the combination band with D_{11}, this is different to the 617 cm^{-1} band discussed above via the D_{20} $\{0,3(-)\}^-$. We also see a ZEKE band at 155 cm^{-1}, which is almost at the same wavenumber as the just-assigned band corresponding to a transition to D_{20} $\{0,3(+)\}^+$ (see above), and assignment to this level does not seem to fit on symmetry grounds, and this is currently only a tentative assignment of this feature. Unfortunately, the signal-to-noise is not good enough to discern the Δv = -1 or $\Delta\{m_1, m_2\}$ = -3 bands corresponding to the main ZEKE feature, which were common features in the *p*FT ZEKE spectra,[13] but the assignment of the $\Delta(v,m)$ = 0 band is relatively straightforward.

In Figure 8(f) the ZEKE spectrum obtained when exciting at 211 cm^{-1} is presented, which shows just two bands, one at 203 cm^{-1} and one at 643 cm^{-1}. An assignment of the ZEKE bands to the $2D_{20}$ and $D_{11} + 2D_{20}$ "pure" vibrational bands is facile, leading to the assignment of the REMPI transition as 20_0^2. (Recalling that four vibtor transitions involving the "cold" torsional levels

will be coincident for all "pure" totally-symmetric vibrational bands.) Blease et al.[24] also saw a band in their REMPI spectra at 211 cm^{-1} but this was unassigned.

A weak band at 338 cm^{-1} appears to be present in this ZEKE spectrum, and this would be consistent with an assignment to 14_0^1. The presence of this (symmetry-forbidden) band in ZEKE spectra of toluene[5] and *p*FT[13] has been reported previously.

7. Excitation via vibtor levels involving D_{19}

We now move onto the next higher pair of bands in the REMPI spectrum, which are highlighted in Figure 9(a), the second of these appears to be a split band (see expanded trace in insert to Figure 9(a)). We have recorded ZEKE spectra via the lowest band at 227 cm^{-1} (Figure 9(b)) and at two positions of the split band, at 254 cm^{-1} and 255 cm^{-1} Figs 9(c) and 9(d). The latter two spectra show the same single feature across the wavenumber range scanned, similar to what was seen in the corresponding case for D_{20}. For the lower wavenumber level, only the region around the expected $\Delta(v,m) = 0$ band was scanned, since the corresponding REMPI feature was very weak; a ZEKE band at 248 cm^{-1} was observed. Together with the calculated vibrational wavenumbers, the REMPI band could be assigned as a transition D_{19} {0,2} ← {0,1}, which are both of *g*″ symmetry; this then assigns the 248 cm^{-1} ZEKE band to the cation D_{19} {0,2} level. Although $\Delta\{m_1, m_2\} = -3$ and $\Delta v = -1$ bands would be expected, no such bands could be discerned, owing to the poor signal-to-noise.

To assign the apparently split REMPI band at 254 cm^{-1}, we note that it is expected to be a transition to a vibtor level involving the D_{19} vibration, with its intensity suggesting it is totally symmetric. By analogy with a similarly observed band in *p*FT, and considering the symmetry of the D_{19} vibration and corresponding vibtor levels (see Table XI), we assign the transition as D_{19} $\{0,3(-)\}^+ \leftarrow \{0,0\}$. With the assumption of the "$\Delta(v,m) = 0$" propensity rule the ZEKE band at 279 cm^{-1} may be assigned as arising from the cation D_{19} $\{0,3(-)\}^+$ level. These values indicate a cation D_{19} vibrational wavenumber of ~233–236 cm^{-1} and a corresponding S_1 value of 211–214 cm^{-1}; these values are both in good agreement with calculated values.[21] Again, no $\Delta\{m_1, m_2\} = -3$ and $\Delta v = -1$ bands could be discerned with the achieved signal-to-noise.

Returning to the split nature of the band at 254 cm^{-1}, we note that exciting from the S_0 {0,1} level could access the D_{19} {3,1}, D_{19} {-3,1} and {0,4} levels, all of which have *g*″ symmetry and

all of which are expected to have very similar transition energies as for the D_{19} $\{0,3(-)\}^{+} \leftarrow \{0,0\}$ transition. In addition, there are corresponding vibtor transitions involving the D_{20} which will have the same symmetry. Hence, in line with comments made above, the splitting in the 254 cm^{-1} and 135-138 cm^{-1} bands could be in line with interactions between the two sets of D_{20} and D_{19} vibtor levels, with the two different symmetries having a slightly different interaction. Another plausible explanation is that interactions with the $2D_{20}$ {0,0} and $2D_{20}$ {0,1} levels is causing the splitting, with the interaction with the D_{19} levels being the stronger, so causing the $2D_{20}$ band to lower in wavenumber; we note that there is no obvious splitting in the $2D_{20}$ band, however, and so it seems likely there are multiple vibronic interactions occurring across the 130–260 cm^{-1} region.

The band at 254 cm^{-1} was observed by Blease et al.,[24] but not assigned.

V. SUMMARY AND CONCLUDING REMARKS

For the first time the spectroscopy of *p*Xyl has been considered in detail using a molecular symmetry group approach. This indicates that the REMPI spectrum consists of a number of overlapping bands, which arise from different torsional levels that cannot be collisionally cooled in a supersonic free jet expansion owing to the different nuclear spin symmetries. This means that in ZEKE experiments, we are exciting from more than one intermediate S_1 level each time. Despite this complication, it is found that the assignment of the REMPI and ZEKE spectra are achievable and that these are very much in line with the assignments of *p*FT[13,14,15] and toluene.[7,8,9] In particular, we have highlighted the similarity of the REMPI spectra in the "pure" torsional region, 0–100 cm^{-1}, for all three molecules, toluene, *p*FT and *p*Xyl, which provides confirmation of the expected similar torsional potentials. More remarkable was the close agreement between the spectra for *p*FT and *p*Xyl in the region 100–200 cm^{-1}, which is where we expect to find vibtor levels involving the D_{20} vibration.[13,14,15] The suggestion is, therefore, that the D_{20} vibrational wavenumber is very similar in both molecules, in agreement with quantum chemical calculations,[21] as are the low wavenumber vibration-torsional interactions. Above 200 cm^{-1} there are deviations in the two spectra, which is in line with this region being associated with vibtor levels that involve the D_{19} vibration, which is expected to lower in wavenumber[21] in *p*Xyl. The unexpected shift in the position of the band

associated with $2D_{20}$ (given that vibtor levels involving this vibration had not shifted significantly) suggested interaction with the higher D_{19} $\{0,3(-)\}^+$ vibtor level; further, a splitting of the D_{20} $\{0,3(-)\}^-$ band and a similar splitting in the D_{19} $\{0,3(-)\}^+$ band suggest that these bands consist of different interacting levels, consistent with both a_1' and g'' contributions from the different cold torsions, and that these are also involved in interactions in this region.

The close agreement also extends to the ZEKE spectra with regard to the activity seen in *p*FT[13] and for *p*Xyl in the present paper. To emphasise this, in Figure 10 we show the 0–600 cm^{-1} regions of the ZEKE spectra of *p*FT and *p*Xyl when exciting through the origin band. As may be seen, the level of agreement of the activity seen in the two cases, bearing in mind the slightly different notation required for the torsional levels in the two molecules, is striking. Using point group symmetry, we see an intense origin and D_{11} band in both cases, but also sizeable bands arising from non-totally symmetric vibrations, D_{14} (a_2, a_u) and D_{19} (b_1, b_{2g}). We also see weak bands from D_{28} and D_{29} (b_2, b_{3g}) for both molecules, but only a weak D_{30} (b_2) band in the case of *p*FT, with this vibration being of b_{2u} symmetry in the case of *p*Xyl. Further comments on the vibrational activity will be provided in ref. 21.

In line with initial discussion by Parmenter and coworkers,[1] and more recently by Lawrance and coworkers,[8,9] it is becoming clear that vibration-torsion coupling pervades the spectra of methyl-substituted molecules and so provides a mechanism by which accelerated internal energy flow is possible. What will be interesting to determine, is the effect of the presence of a second methyl rotor and (longer term) whether the position of this second methyl is important or not in enhancing coupling and so accelerating IVR in the higher wavenumber levels. In the low-wavenumber region examined here, these effects are not so evident but we are currently analysing REMPI and ZEKE spectra of *p*FT and *p*Xyl in the higher-wavenumber region. In the accompanying paper,[21] we show that similar couplings of vibrations and vibtor levels occur in the 400–440 cm^{-1} region as seen for *p*FT[13], but it is clear that the details can vary from molecule to molecule as levels shift in and out of resonance, owing to structural changes in the molecules.

Supplementary Material

See supplementary material for the direct product table for the G_{72} molecular symmetry group.

Acknowledgments

We are grateful to the EPSRC for funding (Grant L021366/1). The EPSRC and the University of Nottingham are thanked for a studentship to W.D.T. We are grateful to the NSCCS for the provision of computer time under the auspices of the EPSRC, and to the High Performance Computer resource at the University of Nottingham. Useful discussions with Warren Lawrance and Jason Gascooke (Flinders University) are gratefully acknowledged.

APPENDIX A. ENERGY LEVELS AND NUCLEAR SPIN STATES FOR A SINGLE ROTOR SYSTEM

1. Energy levels

Molecules containing methyl groups undergo some internal motions that may be considered as torsions. These are also often termed (hindered) internal rotations and these terms are used largely interchangeably in the literature, depending on the context and emphasis.

For a methyl group attached to an infinite mass, the energies, E_{tor}, of the internal rotor/torsional levels are given by

$$E_{tor} = \underline{m}^2 F \tag{A.1}$$

where $\underline{m}$ is the torsional quantum number for an unhindered rotor and is integral, and each level (except for $\underline{m} = 0$) is doubly degenerate; [8,38] F is the rotational constant of the methyl group. In a real molecule, torsion of the methyl group must be counteracted by rotation of the rest of the molecule in the opposite direction, and this slightly changes the rotational constant. This may simply be accounted for by noting that F is an effective rotational constant associated with the torsional motion and includes both the motion of the methyl group and the contrarotary motion of the phenyl ring. Once we have hindered rotation, such as in the molecules toluene and *p*FT, the $\underline{m} = 3$ and $\underline{m} = 6$ levels lose their degeneracy and, following Gascooke et al.,[8] the internal rotor states are now represented by quantum numbers, m. If m is not a multiple of 3, then the levels are still doubly degenerate, but each component could be separately referred to with a +/- sign. If m is a multiple of 3, then new eigenstates are formed, which can be represented[8] as $m = 3(+)$ and $m = 3(-)$, with the sign indicating the specific linear combination of the original $\underline{m} = +3$ and $\underline{m} = -3$ states. These m levels are solutions to the hindered rotor Schrödinger equation:

$$[T_N(\tau) + V(\tau)]\phi_{im}(\tau) = E_{im}\phi_{im}(\tau), m = 0, \pm 1, \pm 2 \ldots \tag{A.2}$$

Here τ is the torsional angle and $V(\tau)$ is the potential energy function; if $V(\tau)$ is expressed as a Fourier series of terms with coefficients, V_n,[39] the first non-trivial term is V_6 for molecules such as toluene and *p*FT, representing the six-fold symmetric potential energy function of the

hindered rotation of the methyl group. The sign of V_6 determines the ordering of the 3(+) and 3(-) levels, and we use the standard definition of τ, such that $V_6 > 0$ corresponds to an eclipsed geometry, with one of the methyl C–H bonds in the same plane as the phenyl ring. [39] The corresponding eigenfunctions, $\phi_{im}(\tau)$, have definite symmetries in the appropriate molecular symmetry group (MSG).[41,42] For toluene and for *p*FT, the MSG is usually termed G_{12}, which is isomorphic to the point group D_{3h}; however, for consistency with the present work, we note that the MSG for toluene and *p*FT can also be termed [3]C_{2v}, indicating the MSG formed from a threefold rotor attached to a C_{2v} point group framework. The character table for G_{12} is presented in Table XII, where the symmetry operations have been expressed in terms of permutation-inversion (PI) operations involving the hydrogen atoms only, which are sufficient to define the group; the behaviour of the C atoms may be deduced from the hydrogen operations. The numbering for the hydrogen atoms is given in Figure 1(a) for toluene; in the case of *p*FT, the fluorine does not add nor detract from the symmetry and so the same character table and PI operations are sufficient to define its symmetry. We note that this table is based on Table A-24 of ref. 41, with the same principal axis system.

For toluene and other *para*-disubstituted benzene molecules with a single rotor, [39,40] we expect to see Δm = 0 transitions (i.e. ones where the torsion quantum number *m* does not change during the transition) as the most intense torsional transitions, followed by Δm = 3 and then Δm = 6 ones and so on. These rules arise from a consideration of an expansion of the transition dipole moment in terms of the torsion angle of a rapidly converging Fourier series and a consideration of the symmetries of each term[39,40] (see below); i.e. they result from electronic-torsional coupling, which may be viewed as a generalized form of Herzberg-Teller coupling. [39]

In a simple perturbation treatment, the splitting between the *m* = 3(+) and *m*= 3(-) levels is equal to $V_6/2$, centred about the unperturbed position, with the ordering of the two levels determined by the sign of V_6. However, the reanalysis of the low-wavenumber region of the spectrum of toluene[8,9] in terms of vibration-torsion coupled levels has led to reassessments of the barriers to internal rotation, lowering the value dramatically in the S_1 state of toluene and resulting in a change in sign for the S_0 state; there is thus the expectation that such interactions also occur in *p*Xyl. This is important, since additional transitions may be seen and

observed transitions could be at shifted positions with respect to those determined by the unperturbed torsional potential and/or unperturbed vibrational levels.

2. Nuclear Spin States

At this point it is pertinent to note that it is often stated (see ref. 23, for example) that the two lowest, m = 0 and m = 1 levels have nuclear spin wavefunctions of different symmetries (*a* and *e*), and these cannot interconvert in a supersonic jet expansion; as a consequence, both m = 0 and m = 1 levels are still populated in such experiments. However, the reasoning behind the above statement, which does not refer to complete G_{12} symmetry labels, is not usually presented in detail, with that of Walker et al. [39] being the most instructive. Since we shall also need to look at this issue for *p*Xyl, we first examine the nuclear spin issue in detail for single-rotor cases such as toluene and *p*FT.

We describe the construction of Table XIII, which shows the allowed symmetries of the various wavefunctions that combine to give an overall allowed Γ_{tot}, which is the symmetry of the overall, or total wavefunction, Φ_{tot}.[41,42] This overall wavefunction includes the symmetry of the electronic motion, the vibrations, torsions and rotations and the nuclear spin functions. We shall include the electronic motion, vibrations and rotations together as ϕ_{evr}, considering the electronic and different nuclear motions as separable, and then consider the torsions (ϕ_{tor}) and nuclear spin functions (ϕ_{ns}) separately; thus:

$$\Phi_{tot} = \phi_{evr}\,\phi_{tor}\,\phi_{ns} \qquad \text{(A.3)}$$

First, Φ_{tot} must be antisymmetric with respect to interchange of odd numbers of pairs of H atoms, and symmetric with respect to even numbers. For the following discussion, the reader is referred to Table XII, which is the character table for the [3]C_{2v} MSG, applicable to molecules such as toluene and *p*FT (adapted from the G_{12} table in ref. 41). We see that the only two allowed symmetries for Φ_{tot} are A_1' and A_2', by considering the operations (123) and (ab)(cd), which both are permutations of even numbers of pairs of hydrogens.

Second, toluene is an asymmetric rotor and hence has sets of rotational levels whose symmetries depend on the K_aK_c labels that fall into even (*e*) and odd (*o*) combinations: *ee*, *eo*, *oe*, *oo*. These can be shown to have symmetries A_1', A_2', A_1'' and A_2'', respectively. We additionally note that in our experiments and analysis we are: (i) working under jet-cooled conditions and hence only the vibrational ground state, (i.e where all of the vibrational quantum numbers are zero, which has an overall symmetry of a_1') has significant population; (ii) assuming the Born-Oppenheimer approximation (where electronic and nuclear motions are separable); (iii) assuming the torsional motion is separable from the vibrational motions, and each of these are separable from rotational motion; and (iv) exciting from the S_0 state which has A_1' symmetry. These considerations mean that the symmetries of ϕ_{evr} will be the same as the symmetries of the asymmetric rotor functions.

Third, the symmetries of the lowest *m* levels in G_{12} are known[39,40] and are given in Figure 2; sometimes, the symmetries have been used with the value of *m* to label the torsional levels in earlier work. We note that since neither ϕ_{evr} nor Γ_{tot} has either *e*′ or *e*″ symmetry functions, then for cases where ϕ_{tor} has these symmetries, then ϕ_{ns} must also have one of the *e*′/*e*″ symmetries to give a total symmetry, Γ_{tot}, of A_1' and A_2'. Lastly, the symmetries of the ϕ_{ns} can be derived as:

80 A_1' + 0 A_2' + 48 A_1'' + 0 A_2'' + 40 E' + 24 E''

This leads to the following spin weights for $\phi_{evr}\phi_{tor}$ functions when combined with the appropriate ϕ_{ns}:

80 for A_1', A_2' and E', 48 for A_1'', A_2'' and E''

Table XIII is therefore constructed by entering the four ϕ_{evr} symmetries and for each of these noting which combinations of ϕ_{tor} and ϕ_{ns} yield an overall Γ_{tot} that is one of A_1' or A_2'. We designate a required ϕ_{ns} that is not available in square brackets. We see from Table XIII that, for example, *m* = 2 (*e*′) levels that have ϕ_{ns} = *e*″ and ϕ_{evr} = a_1'' or a_2'', respectively, can be collisionally cooled to *m* = 1 (*e*″) levels that also have ϕ_{ns} = *e*″ but ϕ_{evr} = a_1' or a_2', respectively; similar arguments hold for *m* = 2 levels with *e*′ ϕ_{ns} functions. Further, we see that it is *not* possible for *m* = 2 levels to cool to the *m* = 0 level, as there are no appropriate ϕ_{evr} *e*′/*e*″ states, and these would be needed to produce an acceptable Γ_{tot} overall.

We can also see, for example, that m= 3(+) (a_1'') levels with ϕ_{ns} = a_1'' and ϕ_{evr} = a_1' or a_2', respectively, can be collisionally cooled to m = 0 (a_1') levels also with ϕ_{ns} = a_1'' and ϕ_{evr} = a_1'' or a_2'', respectively (and *vice versa)*. Further, we see that it is *not* possible for m = 3(+) levels to cool to the m = 1 level, as there are no appropriate ϕ_{evr} = e'/e'' states, which would be needed to produce an acceptable Γ_{tot} overall; again, similar arguments hold for other levels. Variations on these arguments hold for higher m levels, but note also that pre-supersonic jet expansion thermal populations would be low in these cases. In conclusion, therefore, each of the higher (thermally populated) m levels can collapse into one of the m = 0 and m = 1 levels via collisional cooling in the free jet expansion conditions of our experiments. Below we shall discuss similar arguments for a two-rotor system such as *p*Xyl where the situation is slightly more complicated.

APPENDIX B. NUCLEAR SPIN STATES FOR A TWO-ROTOR SYSTEM

The spin statistical weights of the rovibronic-internal rotor states were determined for *p*Xyl consisting of the following isotopes ^{12}C and ^{1}H. The ten ^{1}H atoms give rise to 2^{10} = 1024 ^{1}H-spin functions which belong to the irreducible representations as shown in Table IV and noted below. The sum of the products of the numbers in the column labelled #NS, each combined with the dimension of the respective irreducible representation, is 1024.

As with G_{12} (see Appendix A.2) and with the same assumptions noted there, we construct Table XIV, which shows the allowed symmetries of the various wavefunctions that give an overall allowed Γ_{tot}, which is the symmetry of the total wavefunction, Φ_{tot}. First, as we discussed for [3]C_{2v} above, we note that Φ_{tot} must be antisymmetric with respect to interchange of odd numbers of pairs of H atoms, and symmetric with respect to even numbers. Because the ^{1}H nuclei are fermions, it may be seen here that Φ_{tot} must be symmetric and antisymmetric with respect to the symmetry operators, D and T, respectively. Thus, the allowed symmetry species for the total wavefunction are 00_g^{-+} (A_2') and 00_g^{--} (A_4'), respectively – where the labels in parentheses are the G_{72} labels noted above. Second, the symmetries of ϕ_{evr} will be the same as the symmetries of the asymmetric rotor functions, noted above and given in Table IV. Third, we know that the symmetries of the four lowest {m_1, m_2} levels are: {0,0} (a_1'); {0,1} (g''); {1,1} (e_3'); and {1,-1} (e_1') – see Table IV. In completing Table XIV we note that since ϕ_{evr} does not have any of the e_i', e_i'', g' or g'' symmetry functions,

and that nor does Γ_{tot}, then for cases where ϕ_{tor} has these symmetries, then ϕ_{ns} must also have one of the appropriate e_1', e_2', e_1'', e_2'', g' or g'' symmetries. Lastly, we note that the symmetries of the ϕ_{ns} can be derived as (see Table IV):

88 A_1' + 72 A_4' + 24 E_3' + 16 E_4' + 24 E_1' + 16 E_2' + 80 G' + 48 A_1'' + 48 A_4'' + 12 E_3'' + 12 E_4'' + 12 E_1'' + 12 E_2'' + 48 G''

We start by entering the four permitted ϕ_{evr} symmetries and for each of these consider which combinations of ϕ_{tor} and ϕ_{ns} yield an overall Γ_{tot} that is one of A_2' and A_4'. We designate a required ϕ_{ns} that is not available in square brackets.

First, we consider the lowest {m_1, m_2} levels that might be expect from combinations of m_i = 0 and 1: the {0,0}, {0,1} and {1,1} levels. These may be seen to have different nuclear spin symmetries and hence cannot interconvert in a supersonic jet expansion – they will all therefore survive and be present in our experiment. However, we can also see that the {1,-1} level cannot be cooled to any of these three levels, and hence also survives the expansion in our experiments: it has e_1' torsional symmetry and the permitted nuclear spin symmetries are all different from those of the other three states. On the other hand, the {0,2} level (g' torsional symmetry) can be cooled to the {0,1} level, with a change in rotational level symmetry, while the {0,3}$^{++}$ level (a_1'' torsional symmetry) also does not appear to be able to cool to a lower level, and this is true for some other levels; however, it is likely that only the four lowest levels will be present in the experiment to any significant extent, since pre-supersonic jet expansion thermal population of levels with m_i > 2 will be small.

APPENDIX C.

1. Comments about the {m_1,m_2} states

We have already noted that when one of m_1 and m_2 is divisible by 3, and the other not, such as {0,1}, the four functions are exactly degenerate and such a set belongs to one of the 01 (G) symmetry species. In such levels, the molecule exists in all four of the separate levels simultaneously unless further interactions are brought to bear. To take the specific case of {0,1}, which contains |0,1>, |0,-1>, |1,0> and |-1,0> , one may loosely think of the individual

components as being associated with each methyl group rotating with one quantum of excitation in either direction; however, in reality, actual eigenstates are isoenergetic linear combinations of all of these and both methyl groups are thus rotating, as demanded by the molecular symmetry of the molecule.

When both m_1 and m_2 are multiples of 3, such as |0,3> or |0,6>, the allowed kinetic and potential energy terms create interactions between all members of the set, splitting them up into four energetically-separate levels; to first order their eigenfunctions are linear combinations of all members of the set that can be classified by the characters of the linear combination under the operators *T*, *U* and *S*. These four linear combinations transform like the 00_g (A_i') or the 00_u (A_i'') species (i = 1–4).

If neither m_1 or m_2 are divisible by 3, such as |1,4> or |1,-4>, kinetic and potential energy terms create interactions within the set, but only such that the energy splits into 2 different levels, each doubly degenerate. Each wavefunction can be classified with respect to the character under the operators *T* or *U*; to first order, they are linear combinations of just 2 of the 4 functions in the set. The two pairs of eigenfunctions transform as E_i' or E_i''(i = 1–4). Specific combinations are given in Table V for the various sets given in Table IV.

Here are 3 illustrative examples:

A. For the set {1,4} where σ_1 = 1, σ_2 = 1, the functions (|1,4> + |4,1>)/√2 and (|-4,-1> + |-1,-4>)/√2 are the degenerate functions belonging to the 11_u^+ (E_3'') species, whereas (|1,4> - |4,1>)/√2 and (|-4,-1> - |-1,-4>)/√2 belong to 11_u^- (E_4'').

B. For the set {1,-4} where σ_1 = 1, σ_2 = 2, the functions (|1,-4> + |4,-1>)/√2 and (|-4,1> + |-1,4>)/√2 are the degenerate functions belonging to 12_u^+ (E_1'') species, whereas (|1,-4> - |4,-1>)/√2 and (|-4,1> - |-1,4>)√2 belong to 12_u^- (E_2'').

C. As an example of how these ideas can be extended, for the set {1,7}, one may just substitute 4 by 7 in A) above. The only difference is that the functions now belong to 11_g^+ (E_3') or 11_g^- (E_4'), because $|m_1|+|m_2|$ is now even.

2. {0, m} states for m = 0 modulo 3 (m ≠0)

To draw a comparison with the single-rotor states, it will prove insightful to express the {0, 3}, states for the two-rotor system in a different way to that given in Table IV. If we consider *m* = 3, then, from Table V, there are four {0,3} states:

$$\{0,3\}^{++} = \frac{1}{2}[(0,3)+(3,0)+(0,-3)+(-3,0)]$$

$$\{0,3\}^{+-} = \frac{1}{2}[(0,3)+(3,0)-(-3,0)-(0,-3)]$$

$$\{0,3\}^{-+} = \frac{1}{2}[(0,3)-(3,0)+(-3,0)-(0,-3)]$$

$$\{0,3\}^{--} = \frac{1}{2}[(0,3)-(3,0)-(-3,0)+(0,-3)]$$

(C.1)

If we label the rotor states based on each of the two methyl groups, 1 and 2, as:

$3(+)_1$, $3(-)_1$, $3(+)_2$ and $3(-)_2$

with

$$3(+)_1 = \frac{1}{\sqrt{2}}[(3,0)+(-3,0)]$$

$$3(-)_1 = \frac{1}{\sqrt{2}}[(3,0)-(-3,0)]$$

$$3(+)_2 = \frac{1}{\sqrt{2}}[(0,3)+(0,-3)]$$

$$3(-)_2 = \frac{1}{\sqrt{2}}[(0,3)-(0,-3)]$$

(C.2)

Then it is easy to see that, subject to normalization, the following relations hold:

$$\{0,3\}^{++} = 3(+)_1 + 3(+)_2$$

$$\{0,3\}^{+-} = 3(-)_1 + 3(-)_2$$

$$\{0,3\}^{-+} = 3(-)_2 - 3(-)_1$$

$$\{0,3\}^{--} = 3(+)_2 - 3(+)_1$$

(C.3)

So, the first and fourth levels are +/- linear combinations of 3(+) levels on each centre, which we can denote $\{0,3(+)\}^+$ and $\{0,3(+)\}^-$, respectively; while the second and third levels are +/- linear combinations of 3(-) levels on each centre, which we can denote $\{0,3(-)\}^+$ and $\{0,3(-)\}^-$, respectively. An analogous analysis can be performed for the various {0,6} levels. This notation will be useful for comparing to the single-rotor examples later in the present work.

APPENDIX D. SELECTION RULES FOR A ONE-ROTOR SYSTEM

For a single rotor, the electric dipole transition moment (EDTM) for a pure torsional transition can be written as:

$$\boldsymbol{\mu} = \langle m' | \langle \psi_1(\boldsymbol{q};\tau) | \boldsymbol{\mu} | \psi_0(\boldsymbol{q},\tau) \rangle | m'' \rangle$$

(D.1)

where m' represents the internal rotor quantum number in the upper electronic state; m'' represents that in the lower electronic state; $\boldsymbol{\mu}$ is the electric dipole moment operator; τ is the torsional angle; and $\boldsymbol{q}$ represents the electronic coordinates. With the defined axis system (see Figure 2), the components of $\boldsymbol{\mu}$ transform as T_a, T_b, and T_c, and hence in G_{12} this is as A_1', $A_1''$and A_2'' (see Table XII). The G_{12} symmetries of the S_1 and S_0 electronic states are A_1'' and A_1', respectively, and so the middle integral will transform as a_1'', a_1' and a_2' for $\boldsymbol{\mu_a}$, $\boldsymbol{\mu_b}$ and $\boldsymbol{\mu_c}$, respectively. The next stage is to identify the symmetries of the first few terms in the Fourier transform; these will be sine and cosine terms of 3τ and 6τ and the symmetries of these are given in Table XV. The Fourier transform will have coefficients associated with each term, C_i. Equating each trigonometric term with each dipole moment component by symmetry we get:

$$\mu^a(\tau) = C_3{}^a\cos 3\tau \ (a_1'' \text{ symmetry})$$

$$\mu^b(\tau) = C_0{}^b + C_6{}^b\cos 6\tau \ (a_1' \text{ symmetry})$$

$$\mu^c(\tau) = C_6{}^c\sin 6\tau \ (a_2' \text{ symmetry})$$

(D.2)

For $m'' = 0$, the symmetry is a_1', and so possible values of m' that give an overall totally symmetric EDTM are: *a*-type, $m' = 3(+)$; *b*-type: 0, 6(+); and *c*-type: 6(-). We expect $\Delta m = 0$ transitions to be driven by the C_0 term and be strong, those driven by C_3 terms ($\Delta m = 3$) to be moderately intense, and those driven by C_6 terms to be weak. (Those driven by higher terms will be exceptionally weak and not observable in our spectra.) The $m' = 3(+)$ band gains intensity via electronic-torsional interaction, which is analogous to HT vibronic interaction; this interaction corresponds to that which allows b_2 vibrations to steal intensity from a higher-lying A_1 symmetry state in the spectra of C_{2v} point group symmetry substituted benzenes.

For $m'' = 1$, the symmetry is e'' and so possible values of m' that give an overall totally symmetric EDTM are: *a*-type: $m' = 2, 4$; *b*-type: 1,5; and *c*-type: $m' = 1,5$. The $\Delta m = 0$ transition to $m' = 1$ will be intense, the $\Delta m = 3$ transition to $m' = 2$ (remembering m is signed) will be weak, and the $\Delta m = 6$ transition to $m' = 5$ will be very weak.

For the $\tilde{X}^2A_2''$ (D_0^+) $\leftarrow$ $\tilde{A}^1A_1''$ (S_1) transition, the symmetries of the electronic states now mean that the "middle" integral will have symmetries $a_2'' \times (a_1', a_1'', a_2'') \times a_1'' = a_2', a_2''$ and a_1'', corresponding to *a*-, *b*- and *c*-type transitions, respectively. This means that, when exciting from the $m'' = 0$ level (and disregarding the symmetry of the departing Rydberg electron), we can access the 6(-), 3(-) and 3(+) states, respectively (see left-hand side of Figure 2) through an electronic-torsional coupling mechanism. The second and third of these will be weak, while the first will be very weak, being a $\Delta m = 6$ transition. However, it is possible for the $\Delta m = 3$ transitions to steal oscillator strength from higher lying electronic states, analogous to the HT intensity stealing mechanisms of vibrations, see below. Hence the relative intensity of 3(+)/3(-) in photoelectron/ZEKE spectra depends on the proximity of higher states of the

correct symmetry from which intensity can be stolen – see the discussion in our recent *p*FT ZEKE paper.[13] It should be noted that only the 3(+) level may be observed through electronic-torsion coupling in the S_1 state since there is no component of the TDM of the correct symmetry for the 3(-) state to appear. [39]

Table I: Generating symmetry operators and their effects on space-fixed position vectors [a]

Operator	C_1	C_2	T	S	D
Order	3	3	2	2	2
$\alpha \rightarrow$	α	α	$\alpha + \pi$	$\alpha + \pi$	α
$\beta \rightarrow$	β	β	$\pi - \beta$	$\pi - \beta$	β
$\gamma \rightarrow$	γ	γ	$-\gamma$	$\pi - \gamma$	$\gamma + \pi$
$\tau_1 \rightarrow$	$\tau_1 - \omega$	τ_1	τ_2	$-\tau_1$	$\tau_1 - \pi$
$\tau_2 \rightarrow$	τ_2	$\tau_2 - \omega$	τ_1	$-\tau_2$	$\tau_2 - \pi$
$X_{j,l} \rightarrow$	$X_{j,l}$	$X_{j,l}$	$X_{3-j,3-l}$	$-X_{j,l}$	$X_{j,3-l}$
$X_{1,k} \rightarrow$	$X_{1,k-1}$	$X_{1,k}$	$X_{2,k}$	$-X_{1,-k}$	$X_{1,k}$
$X_{2,k} \rightarrow$	$X_{2,k}$	$X_{2,k-1}$	$X_{1,k}$	$-X_{2,-k}$	$X_{2,k}$
Equivalent rotation	R^0	R^0	R_b^{π}	R_c^{π}	R_a^{π}
PI operator	(123)	(456)	(14)(25)(36)(ac)(bd)	(23)(56)*	(ab)(cd)

[a] The labels 1,2,3 of the methyl H atoms in the permutation inversion operator notation correspond to k = 3, 2, 1 for j = 2. Similarly, the labels 4, 5, 6 correspond to k = 3, 2, 1 for j = 1. For the H atoms on the benzene ring, *a*, *b*, *c*, and *d* correspond to (j, l) = (2,1), (2,2), (1,2) and (1,1), respectively.

Table II: Equivalent permutation inversion (PI) operators of the class representative operators of group [3,3]D_{2h}.

Operator[a]	Equivalent PI operator[b]	Operator[a]	Equivalent PI operator[b]
E	E	D	(ab)(cd)
$C_1C_2^{-1}$	(123)(465)	$C_1C_2^{-1}D$	(123)(465)(ab)(cd)
C_1C_2	(123)(456)	C_1C_2D	(123)(456)(ab)(cd)
C_1	(123)	C_1D	(123)(ab)(cd)
T	(14)(25)(36)(ac)(bd)	TD	(14)(25)(36)(ad)(bc)
C_1C_2T	(153426)(ac)(bd)	C_1C_2TD	(153426)(ad)(bc)
U	(14)(26)(35)(ac)(bd)*	UD	(14)(26)(35)(ad)(bc)*
$C_1C_2^{-1}U$	(163425)(ac)(bd)*	$C_1C_2^{-1}UD$	(163425)(ad)(bc)*
S	(23)(56)*	SD	(23)(56) (ab)(cd)*

[a] See Table II for the effect of the generating symmetry operators on the space-fixed axes.

[b] The letters and numbers refer to Figure 1(b). The PI symbols show only the effects on the H atoms which is sufficient to define the MS group.

Table III: Character table of the molecular symmetry group [3,3]D_{2h} (G_{72})[a]

[3,3]D_{2h}	G_{72}[b]	E	$C_1C_2^{-1}$	C_1C_2	C_1	T	C_1C_2T	U	$C_1C_2^{-1}U$	S	D	$C_1C_2^{-1}D$	C_1C_2D	C_1D	TD	C_1C_2TD	UD	$C_1C_2^{-1}UD$	SD
#[c]		1	2	2	4	3	6	3	6	9	1	2	2	4	3	6	3	6	9
00_g^{++}	A_1'	1	1	1	1	1	1	1	1	1	1	1	1	1	1	1	1	1	1
00_g^{+-}	A_3'	1	1	1	1	1	1	-1	-1	-1	1	1	1	1	1	1	-1	-1	-1
00_g^{-+}	A_2'	1	1	1	1	-1	-1	1	1	-1	1	1	1	1	-1	-1	1	1	-1
00_g^{--}	A_4'	1	1	1	1	-1	-1	-1	-1	1	1	1	1	1	-1	-1	-1	-1	1
11_g^{+}	E_3'	2	2	-1	-1	2	-1	0	0	0	2	2	-1	-1	2	-1	0	0	0
11_g^{-}	E_4'	2	2	-1	-1	-2	1	0	0	0	2	2	-1	-1	-2	1	0	0	0
12_g^{+}	E_1'	2	-1	2	-1	0	0	2	-1	0	2	-1	2	-1	0	0	2	-1	0
12_g^{-}	E_2'	2	-1	2	-1	0	0	-2	1	0	2	-1	2	-1	0	0	-2	1	0
01_g	G'	4	-2	-2	1	0	0	0	0	0	4	-2	-2	1	0	0	0	0	0
00_u^{++}	A_1''	1	1	1	1	1	1	1	1	1	-1	-1	-1	-1	-1	-1	-1	-1	-1
00_u^{+-}	A_3''	1	1	1	1	1	1	-1	-1	-1	-1	-1	-1	-1	-1	-1	1	1	1
00_u^{-+}	A_2''	1	1	1	1	-1	-1	1	1	-1	-1	-1	-1	-1	1	1	-1	-1	1
00_u^{--}	A_4''	1	1	1	1	-1	-1	-1	-1	1	-1	-1	-1	-1	1	1	1	1	-1
11_u^{+}	E_3''	2	2	-1	-1	2	-1	0	0	0	-2	-2	1	1	-2	1	0	0	0
11_u^{-}	E_4''	2	2	-1	-1	-2	1	0	0	0	-2	-2	1	1	2	-1	0	0	0
12_u^{+}	E_1''	2	-1	2	-1	0	0	2	-1	0	-2	1	-2	1	0	0	-2	1	0
12_u^{-}	E_2''	2	-1	2	-1	0	0	-2	1	0	-2	1	-2	1	0	0	2	-1	0
01_u	G''	4	-2	-2	1	0	0	0	0	0	-4	2	2	-1	0	0	0	0	0

[a] $U = TS = ST$

[b] G_{72} species labels adapted from labels of G_{36} (Table A-28 in Ref. 41) since $G_{72} = G_{36} \times \{E, D\}$

[c] # is the number of operators in the class

Table IV: Transformation properties of nuclear spin (NS) functions, free internal rotor functions, asymmetric rotor functions (ASR) and the electric vibronic dipole moment terms.

$[3,3]D_{2h}$	G_{72}	#NS [a]	Free internal rotor functions [b]				[c, d]
			$m \neq n$	$m+n$		$[m_1,m_2\}$ set of lowest energy [e]	
00_g^{++}	A_1'	88	$\{3m,3n\}^{++}$	even	$\{0,0\}$, $\{3m,-3m\}^{+}$, $\{3m,3m\}^{+}$	$\{0,0\}$; $\{3,3\}^{+}$; $\{3,-3\}^{+}$; $\{0,6\}^{++}$	*ee*
00_g^{+-}	A_3'	0	$\{3m,3n\}^{+-}$	even	$\{3m,3m\}^{-}$	$\{3,3\}^{-}$; $\{0,6\}^{+-}$	Γ^*
00_g^{-+}	A_2'	0	$\{3m,3n\}^{-+}$	even	$\{3m,-3m\}^{+}$	$\{3,-3\}^{-}$; $\{0,6\}^{-+}$	*eo*, J_a
00_g^{--}	A_4'	72	$\{3m,3n\}^{--}$	even		$\{0,6\}^{--}$	T_a
11_g^{+}	E_3'	24	$\{3m+1,3n+1\}^{1+}$	even	$\{3m+1,3m+1\}$	$\{1,1\}$; $\{-2,-2\}$; $\{4,-2\}^{+}$; $\{1,-5\}^{+}$; $\{4,4\}$	
11_g^{-}	E_4'	16	$\{3m+1,3n+1\}^{1-}$	even		$\{4,-2\}^{-}$; $\{1,-5\}^{-}$	
12_g^{+}	E_1'	24	$\{3m+1,3n+2\}^{2+}$	odd	$\{3m+1,3m+2\}$	$\{1,-1\}$; $\{-2,2\}$; $\{4,2\}^{+}$; $\{1,5\}^{+}$; $\{4,-4\}$	
12_g^{-}	E_2'	16	$\{3m+1,3n+2\}^{2-}$	odd		$\{4,2\}^{-}$; $\{1,5\}^{-}$	
01_g	G'	80	$\{3m,3n+1\}$	odd		$\{0,2\}$; $\{-3,1\}$; $\{3,1\}$; $\{0,4\}$; $\{3,-5\}$; $\{-3,-5\}$	
00_u^{++}	A_1''	48	$\{3m,3n\}^{++}$	odd		$\{0,3\}^{++}$	T_b
00_u^{+-}	A_3''	0	$\{3m,3n\}^{+-}$	odd		$\{0,3\}^{+-}$	*oo*, J_b
00_u^{-+}	A_2''	0	$\{3m,3n\}^{-+}$	odd		$\{0,3\}^{-+}$	T_c
00_u^{--}	A_4''	48	$\{3m,3n\}^{--}$	odd		$\{0,3\}^{--}$	*oe*, J_c
11_u^{+}	E_3''	12	$\{3m+1,3n+1\}^{1+}$	odd	$\{3m+1,3m+1\}$	$\{1,-2\}^{+}$; $\{1,4\}^{+}$; $\{-2,-5\}^{+}$	
11_u^{-}	E_4''	12	$\{3m+1,3n+1\}^{1-}$	odd		$\{1,-2\}^{-}$; $\{1,4\}^{-}$; $\{-2,-5\}^{-}$	

12_u^+	E_1"	12	$\{3m+1,3n+2\}^{2+}$	even	$\{3m+1,3m+2\}$	$\{1,2\}^+$; $\{1,-4\}^+$; $\{-5,2\}^+$	
12_u^-	E_2"	12	$\{3m+1,3n+2\}^{2-}$	even		$\{1,2\}^-$; $\{1,-4\}^-$; $\{-5,2\}^-$	
01_u	G"	48	$\{3m,3n+1\}$	even		{0,1}; {3,-2}; {-3,-2}; {-3,4}; {0,5}; {3,4}	

[a] #NS indicates the number of nuclear spin functions of each symmetry type.

[b] Each of the different types of functions is defined in Table VI.

[c] *ee*, *eo*, *oo*, *oe* are the parities of the asymmetric rotor eigenfunction, K_aK_c.

[d] Transformation of translational and rotational degrees of freedom designated by $T_{a,b,c}$,and $J_{a,b,c}$, respectively; Γ^* = species of electric dipole transitions in space-fixed axes system.

[e] $\{m_1,m_2\}$ set with lowest energies for this spin function

Table V: Syntax for internal rotor function combinations as employed in Table V

Syntax	Number of degenerate functions	Linear combination
$\{a,b\}^{++}$	1	$(f_{a,b}+f_{b,a}+f_{-b,-a}+f_{-a,-b})/2$
$\{a,b\}^{+-}$	1	$(f_{a,b}+f_{b,a}-f_{-b,-a}-f_{-a,-b})/2$
$\{a,b\}^{-+}$	1	$(f_{a,b}-f_{b,a}+f_{-b,-a}-f_{-a,-b})/2$
$\{a,b\}^{--}$	1	$(f_{a,b}-f_{b,a}-f_{-b,-a}+f_{-a,-b})/2$
$\{a,b\}^{1+}$	2	$(f_{a,b}+f_{b,a})/\sqrt{2}, (f_{-b,-a}+f_{-a,-b})/\sqrt{2}$
$\{a,b\}^{1-}$	2	$(f_{a,b}-f_{b,a})/\sqrt{2}, (f_{-b,-a}-f_{-a,-b})/\sqrt{2}$
$\{a,b\}^{2+}$	2	$(f_{a,b}+f_{-b,-a})/\sqrt{2}, (f_{b,a}+f_{-a,-b})/\sqrt{2}$
$\{a,b\}^{2-}$	2	$(f_{a,b}-f_{-b,-a})/\sqrt{2}, (f_{b,a}-f_{-a,-b})/\sqrt{2}$
$\{a,b\}$	4	$f_{a,b}, f_{b,a}, f_{-b,-a}, f_{-a,-b}$
$\{a,a\}^{+}$	1	$(f_{a,a}+f_{-a,-a})/\sqrt{2}$
$\{a,a\}^{-}$	1	$(f_{a,a}-f_{-a,-a})/\sqrt{2}$
$\{a,-a\}$	2	$f_{a,-a}, f_{-a,a}$
$\{a,-a\}^{+}$	1	$(f_{a,-a}+f_{-a,a})/\sqrt{2}$
$\{a,-a\}^{-}$	1	$(f_{a,-a}-f_{-a,a})/\sqrt{2}$
$\{a,a\}$	2	$f_{a,a}, f_{-a,-a}$

Table VI: Symmetries of Trigonometric Functions for the G_{72} MSG

$\Delta\{m_1, m_2\}$	Trig. function	symmetry
G_{72}		
3	$\cos 3\tau_1 + \cos 3\tau_2$	a_1''
	$\sin 3\tau_1 + \sin 3\tau_2$	a_3''
	$\cos 3\tau_1 - \cos 3\tau_2$	a_4''
	$\sin 3\tau_1 - \sin 3\tau_2$	a_2''
6	$\cos 3\tau_1 \cos 3\tau_2$	a_1'
	$\sin 3\tau_1 \sin 3\tau_2$	a_1'
	$\sin 3\tau_1 \cos 3\tau_2 + \cos 3\tau_1 \sin 3\tau_2$	a_3'
	$\sin 3\tau_1 \cos 3\tau_2 - \cos 3\tau_1 \sin 3\tau_2$	a_2'
	$\cos 6\tau_1 + \cos 6\tau_2$	a_1'
	$\sin 6\tau_1 + \sin 6\tau_2$	a_3'
	$\cos 6\tau_1 - \cos 6\tau_2$	a_4'
	$\sin 6\tau_1 - \sin 6\tau_2$	a_2'

Table VII: Energies of local minima and maxima of potential functions with $V_{6,0} > 0$

Conformation[a]	τ_1, τ_2 Position 1	τ_1, τ_2 Position 2	Type of turning point	Energy	Relative Energy
$C_{2v}(b)$ ee	0, 0	$\pi/3$, $\pi/3$	maximum	$2V_{6,0} + V_{3,3} + V_{3,-3}$	$4V_{6,0} + 2V_{3,3}$
$C_{2h}(c)$ ee	0, $\pi/3$	$\pi/3$, 0	maximum	$2V_{6,0} - V_{3,3} - V_{3,-3}$	$4V_{6,0} - 2V_{3,-3}$
$C_{2v}(c)$ ss	$\pi/6$, $-\pi/6$	$-\pi/6$, $\pi/6$	minimum	$-2V_{6,0} + V_{3,3} - V_{3,-3}$	$2V_{3,3} - 2V_{3,-3}$
$C_{2h}(b)$ ss	$\pi/6$, $\pi/6$	$-\pi/6$, $-\pi/6$	minimum	$-2V_{6,0} - V_{3,3} + V_{3,-3}$	0
	0, $\pm\pi/6$ $\pm\pi/6$, 0	π, $\pm\pi/6$ $\pm\pi/6$, π	saddle point	0	$2V_{6,0} + V_{3,3} - V_{3,-3}$

[a] See text for descriptions of conformation

Table VIII: Hamiltonian matrix for the energy levels of the {0,3} set of internal rotor functions

	|0,3>	|3,0>	|-3,0>	|0,-3>
|0,3>	E_{03}	$V_{3,-3}/2$	$V_{3,3}/2$	$V_{6,0}/2$
|3,0>	$V_{3,-3}/2$	E_{03}	$V_{6,0}/2$	$V_{3,3}/2$
|-3,0>	$V_{3,3}/2$	$V_{6,0}/2$	E_{03}	$V_{3,-3}/2$
|0,-3>	$V_{6,0}/2$	$V_{3,3}/2$	$V_{3,-3}/2$	E_{03}

Table IX: Results for the energies of symmetrized functions for the matrix in Table X

Function	Energy
$\|0,3\rangle + \|3,0\rangle + \|-3,0\rangle + \|0,-3\rangle = \{0,3\}^{++} = \{0,3(+)\}^{+}$	$E_{03} + \frac{1}{2}(V_{3,3}+V_{3,-3}) + V_{6,0}/2$
$\|0,3\rangle - \|3,0\rangle - \|-3,0\rangle + \|0,-3\rangle = \{0,3\}^{--} = \{0,3(+)\}^{-}$	$E_{03} - \frac{1}{2}(V_{3,-3}+V_{3,3}) + V_{6,0}/2$
$\|0,3\rangle + \|3,0\rangle - \|-3,0\rangle - \|0,-3\rangle = \{0,3\}^{+-} = \{0,3(-)\}^{+}$	$E_{03} + \frac{1}{2}(V_{3,-3}-V_{3,3}) - V_{6,0}/2$
$\|0,3\rangle - \|3,0\rangle + \|-3,0\rangle - \|0,-3\rangle = \{0,3\}^{-+} = \{0,3(-)\}^{-}$	$E_{03} - \frac{1}{2}(V_{3,-3}-V_{3,3}) - V_{6,0}/2$

TABLE X: Correspondence between symmetry classes for the D_{2h} point group and the [3,3]D_{2h} MSG; in the case of the latter, the corresponding G_{72} labels are given, as are the corresponding ones for G_{12}

D_{2h}	[3,3]D_{2h}	G_{72}	G_{12}
a_g	00_g^{++}	A_1'	A_1'
b_{1g}	00_g^{-+}	A_2'	A_2'
a_u	00_g^{+-}	A_3'	A_2'
b_{1u}	00_g^{--}	A_4'	A_1'
	12_g^{+}	E_1'	E'
	12_g^{-}	E_2'	E'
	11_g^{+}	E_3'	E'
	11_g^{-}	E_4'	E'
	01_g	G'	$A_1'+A_2' + E'$
b_{2u}	00_u^{++}	A_1"	A_1''
b_{3u}	00_u^{-+}	A_2"	A_2''
b_{2g}	00_u^{+-}	A_3"	A_2''
b_{3g}	00_u^{--}	A_4"	A_1''
	12_u^{+}	E_1"	E''
	12_u^{-}	E_2"	E''
	11_u^{+}	E_3"	E''
	11_u^{-}	E_4"	E''
	01_u	G"	E''

TABLE XI: Symmetries of torsions and vibtor levels involving the lowest three vibrations.

$\{m_1,m_2\}$	Pure or A_1'	$D_{20}(A_2'')$	D_{19} (A_3'')	D_{14} (A_3')
{0,0}	a_1'	a_2''	a_3''	a_3'
{0,1}	g''	g'	g'	g''
{1,1}	e_3'	e_4''	e_3''	e_3'
{1,-1}	e_1'	e_1''	e_2''	e_2'
{0,2}	g'	g''	g''	g'
$\{1,2\}^+$	e_1''	e_1'	e_2'	e_2''
$\{1,2\}^-$	e_2''	e_2'	e_1'	e_1''
$\{1,-2\}^+$	e_3''	e_4'	e_3'	e_3''
$\{1,-2\}^-$	e_4''	e_3'	e_4'	e_4''
$\{0,3(+)\}^+$	a_1''	a_2'	a_3'	a_3''
$\{0,3(+)\}^-$	a_4''	a_3'	a_2'	a_2''
$\{0,3(-)\}^+$	a_3''	a_4'	a_1'	a_1''
$\{0,3(-)\}^-$	a_2''	a_1'	a_4'	a_4''
{3,1}	g'	g''	g''	g'
{-3,1}	g'	g''	g''	g'
{0,4}	g'	g''	g''	g'
$\{1,4\}^+$	e_3''	e_4'	e_3'	e_3''
$\{1,4\}^-$	e_4''	e_3'	e_4'	e_4''
$\{1,-4\}^+$	e_1''	e_1'	e_2'	e_2''
$\{1,-4\}^-$	e_2''	e_2'	e_1'	e_1''
{0,5}	g''	g'	g'	g''
$\{1,5\}^+$	e_1'	e_1''	e_2''	e_2'
$\{1,5\}^-$	e_2'	e_2''	e_1''	e_1'
$\{1,-5\}^+$	e_3'	e_4''	e_3''	e_3'
$\{1,-5\}^-$	e_4'	e_3''	e_4''	e_4'
$\{0,6(+)\}^+$	a_1'	a_2''	a_3''	a_3'
$\{0,6(+)\}^-$	a_4'	a_3''	a_2''	a_2'
$\{0,6(-)\}^+$	a_3'	a_4''	a_1''	a_1'
$\{0,6(-)\}^-$	a_2'	a_1''	a_4''	a_4'
{6,1}	g''	g'	g'	g''
{-6,1}	g''	g'	g'	g''

Table XII: Character table of the MS group [3]C_{2v} (G_{12}) adapted from ref. 41 for molecules such as toluene and *p*FT – See Figure 1(a)

[3]C_{2v}	E	(123)	(23)*	(ab)(cd)	(123)(ab)(cd)	(23)(ab)(cd)*	[a]
[b]	E	C_1	S	D	C_1D	SD	
[c]	1	2	3	1	2	3	
[d]	R^0	R^0	R_c^π	R_a^π	R_a^π	R_b^π	
A_1'	1	1	1	1	1	1	T_a, *ee*
A_1''	1	1	1	-1	-1	-1	T_b, J_c, *oe*
A_2'	1	1	-1	1	1	-1	J_a, *eo*, Γ^*
A_2''	1	1	-1	-1	-1	1	T_c, J_b, *oo*
E'	2	-1	0	2	-1	0	
E''	2	-1	0	-2	1	0	

[a] Transformation of translational and rotational degrees of freedom designated by $T_{a,b,c}$,and $J_{a,b,c}$, respectively; Γ^* = species of electric dipole transitions in space-fixed axes system. *ee*, *eo*, *oo*, *oe* are the parities of K_aK_c, the asymmetric rotor eigenfunction label.

[b] Equivalent operator in [3,3]D_{2h} / G_{72}, with the molecule-fixed axis system identical to that used for G_{72}.

[c] Number of operators in class.

[d] Equivalent rotation.

Table XIII (for Appendix A): Wavefunction symmetry combinations that give an allowed overall symmetry for Φ_{tot} in G_{12}

ϕ_{evr}	ϕ_{tor}	ϕ_{ns}[a]	Γ_{tot}
A_1'	a_1'	a_1'	A_1'
	a_1''	a_1''	
	a_2'	$[a_2']$	
	a_2''	$[a_2'']$	
	e'	e'	
	e''	e''	
	a_1'	$[a_2']$	A_2'
	a_1''	$[a_2'']$	
	a_2'	a_1'	
	a_2''	a_1''	
	e'	e'	
	e''	e''	
A_2'	a_1'	$[a_2']$	A_1'
	a_1''	$[a_2'']$	
	a_2'	a_1'	
	a_2''	a_1''	
	e'	e'	
	e''	e''	
	a_1'	a_1'	A_2'
	a_1''	a_1''	
	a_2'	$[a_2']$	
	a_2''	$[a_2'']$	
	e'	e'	
	e''	e''	
A_1''	a_1'	a_1''	A_1'
	a_1''	a_1'	
	a_2'	$[a_2'']$	
	a_2''	$[a_2']$	
	e'	e''	
	e''	e'	
	a_1'	$[a_2'']$	A_2'
	a_1''	$[a_2']$	
	a_2'	a_1''	
	a_2''	a_1'	
	e'	e''	
	e''	e'	
A_2''	a_1'	$[a_2'']$	A_1'
	a_1''	$[a_2']$	
	a_2'	a_1''	
	a_2''	a_1'	
	e'	e''	
	e''	e'	
	a_1'	a_1''	A_2'
	a_1''	a_1'	
	a_2'	$[a_2'']$	
	a_2''	$[a_2']$	
	e'	e''	
	e''	e'	

[a] Square brackets indicate that these symmetries do not exist and so the corresponding combination of ϕ_{evr} and ψ_{tor} is not allowed.

Table XIV: Wavefunction symmetry combinations that give an allowed overall symmetry for Φ_{tot} in [3,3]D_{2h}

ϕ_{evr}	ϕ_{tor}	ϕ_{ns}[a]	Γ_{tot}
A_1'	a_1'	[a_2']	A_2'
	g''	g''	
	e_3'	e_4'	
	e_1'	e_1'	
	g'	g'	
	a_1''	[a_2'']	
	a_1'	a_4'	A_4'
	g''	g''	
	e_3'	e_4'	
	e_1'	e_2'	
	g'	g'	
	a_1''	a_4''	
A_2'	a_1'	a_1'	A_2'
	g''	g''	
	e_3'	e_3'	
	e_1'	e_1'	
	g'	g'	
	a_1''	a_1''	
	a_1'	[a_3']	A_4'
	g''	g''	
	e_3'	e_3'	
	e_1'	e_2'	
	g'	g'	
	a_1''	[a_3'']	
A_4''	a_1'	[a_3'']	A_2'
	g''	g'	
	e_3'	e_3''	
	e_1'	e_2''	
	g'	g''	
	a_1''	[a_3']	
	a_1'	a_1''	A_4'
	g''	g'	
	e_3'	e_3''	
	e_1'	e_1''	
	g'	g''	
	a_1''	a_1'	
A_3''	a_1'	a_4''	A_2'
	g''	g'	
	e_3'	e_4''	
	e_1'	e_2''	
	g'	g''	
	a_1''	a_4'	
	a_1'	[a_2'']	A_4'
	g''	g'	
	e_3'	e_4''	
	e_1'	e_1''	
	g'	g''	
	a_1''	[a_2']	

[a] Square brackets indicate a combination of ϕ_{evr} and ϕ_{tor} that is not allowed.

Table XV (for Appendix B): Symmetries of Trigonometric Functions for the G_{12} MSG

Δm	Trig. function	symmetry
G_{12}		
3	$\sin 3\tau$	a_2''
	$\cos 3\tau$	a_1''
6	$\sin 6\tau$	a_2'
	$\cos 6\tau$	a_1'

Figure Captions

Figure 1: Numbering of the atoms in (a) toluene and (b) *p*-xylene. These numberings are employed in denoting the effect of the permutation-inversion operations — see text.

Figure 2: Schematics of the axis systems used in the present work are presented at the top of the figure. Below this, on the left-hand side are the correlations between the symmetry classes of the point groups D_{6h} and C_{2v}, and then with those of the G_{12} molecular symmetry group, which can also be denoted [3]C_{2v}. On the right-hand side, are the correlations between the symmetry classes of the point groups D_{6h} and D_{2h} and then with those of the G_{72} molecular symmetry group, which can also be denoted [3,3]D_{2h}. The $\{m_1,m_2\}$ levels are not added to this figure to avoid overcrowding, but their symmetries can be found in Table V. Note that there are no equivalent classes of the various *e* and *g* molecular symmetry classes in the point groups.

Figure 3: Contour plots of potential surfaces with global minima at the $C_{2h}(b)$ and C_{2v}(c) conformations. Dark purple: global minima; dark orange: local maxima. $C_{2h}(b)$ plot: $V_{6,0}$ = 25, $V_{3,3}$ = 15, $V_{3,-3}$ = 1. C_{2v}(c) plot: $V_{6,0}$ = 25, $V_{3,3}$ = 15, $V_{3,-3}$ = 1. C_{2v}(c). The horizontal axis (τ_1) and vertical axis (τ_2) run from $-\pi/3$ to $+\pi/3$ – the numbers are arbitrary energy units.

Figure 4: REMPI spectra of (a) toluene, (b) *p*FT and (c) *p*Xyl in the range 0–350 cm^{-1}. The wavenumber scale is relative to the respective origins, which are located at 37476.8 cm^{-1},[5] 36859.9 cm^{-1},[13] and 36724 cm^{-1} (present work). The assignments of the bands are given as transitions that involve just torsional or a combination of vibration and torsional quantum numbers. Owing to different nuclear spin state symmetries, various initial torsional levels are populated in our free jet expansion (see text), while only the zero-point vibrational level is expected to be populated significantly. For clarity, the lower torsional levels are omitted for *p*Xyl. The assignments in many cases rely on the ZEKE spectra recorded via different intermediate levels, which are presented in subsequent figures and discussed in the text. Hence a number of transitions appear at the same wavenumber, but for clarity these are not all marked here: for example, the origin band, marked 0^0 will consist of two $\Delta m = 0$ excitations from m'' = 0 and 1 for toluene and *p*FT; while for *p*Xyl, the origin band will consist of four $\Delta\{m_1,m_2\} = 0$ transitions from S_0 levels {0,0}, {0,1}, {1,1} and {1,-1} – see text.

Figure 5: (a) REMPI spectrum of *p*Xyl highlighting the "pure" torsions below 100 cm^{-1}. Traces (b)–(e) show the ZEKE spectra recorded when exciting through the S_1 origin band and different S_1 levels as indicated. Assignments are discussed in the text. For clarity, only the terminating torsional levels are shown on the REMPI spectrum.

Figure 6: (a) REMPI spectrum of *p*Xyl emphasising the REMPI feature at ~76 cm^{-1}. Owing to the profile, different excitation wavenumbers were employed. Traces (b)–(d) show the ZEKE spectra recorded at these points, and their assignment is discussed in the text. For clarity, only the terminating torsional levels are shown on the REMPI spectrum.

Figure 7: (a) REMPI spectrum of *p*Xyl emphasising the REMPI feature at ~110 cm^{-1}. Owing to the profile, different excitation wavenumbers were employed as shown in the insert in (a), with the main trace indicating the position of the band in the REMPI spectrum. Traces (b)–(d) show the ZEKE spectra recorded at these points, and their assignment is discussed in the text.

Figure 8: (a) REMPI spectrum of *p*Xyl emphasising levels involving the D_{20} vibration. Traces (b)–(e) show the ZEKE spectra recorded using the indicated S_1 level as the excitation step. The intermediate levels are shown on the right-hand side of each trace, and just the terminating levels of the ionization step are indicated on each band.

Figure 9: (a) REMPI spectrum of *p*Xyl emphasising levels involving the D_{19} vibration; the insert shows an expansion of the band at ~ 254 cm^{-1}, which appears to be split – see text. Traces (b), (c) and (d) show the ZEKE spectra recorded using the indicated S_1 level as the excitation step. The intermediate levels are shown on the right-hand side of each trace, and just the terminating levels of the ionization step are indicated on each band.

Figure 10: Expanded views and assignments of the 0–600 cm^{-1} regions of the ZEKE spectra of (a) *p*Xyl and (b) *p*FT, obtained when exciting via the S_1 origin band. The vertical scale has been expanded compared to traces for *p*Xyl shown in other spectra. The similarity between the spectral activity and assignments is noteworthy.

Figure 1

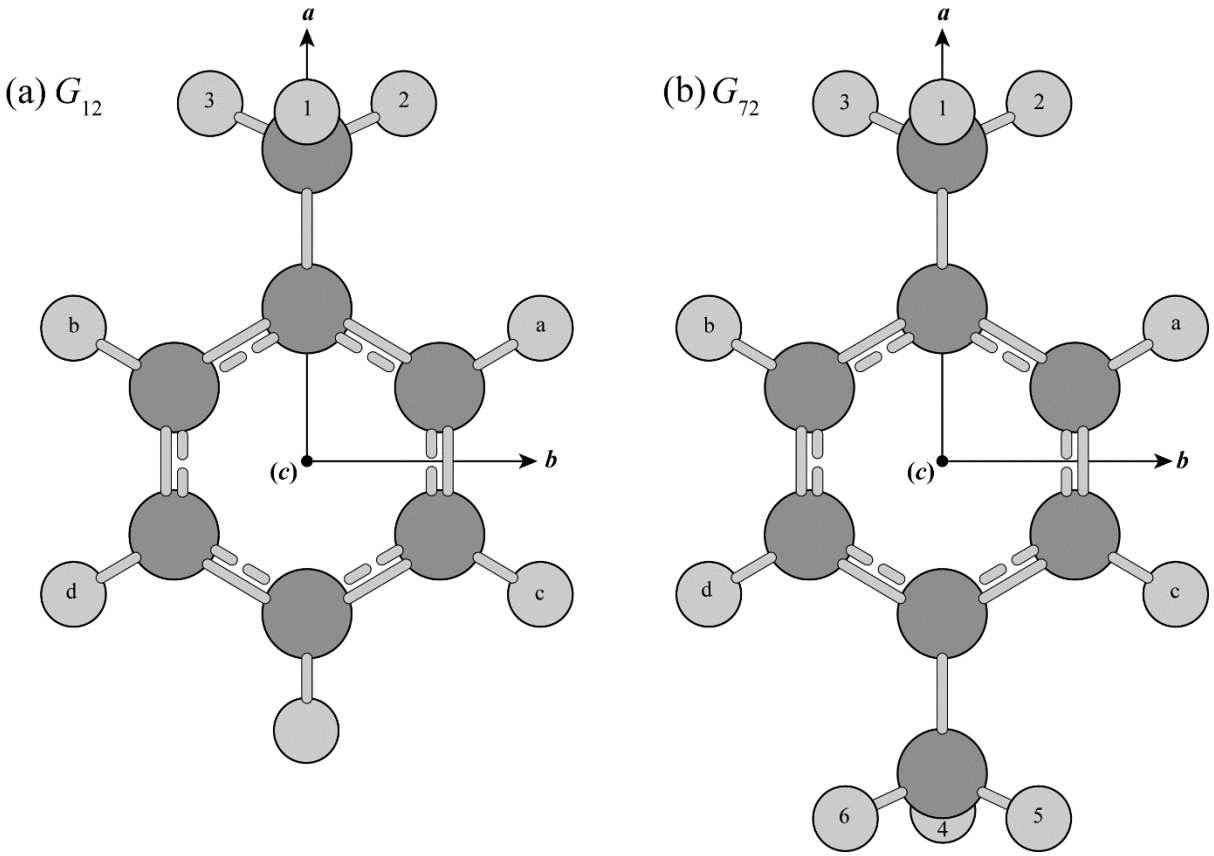

Figure 2

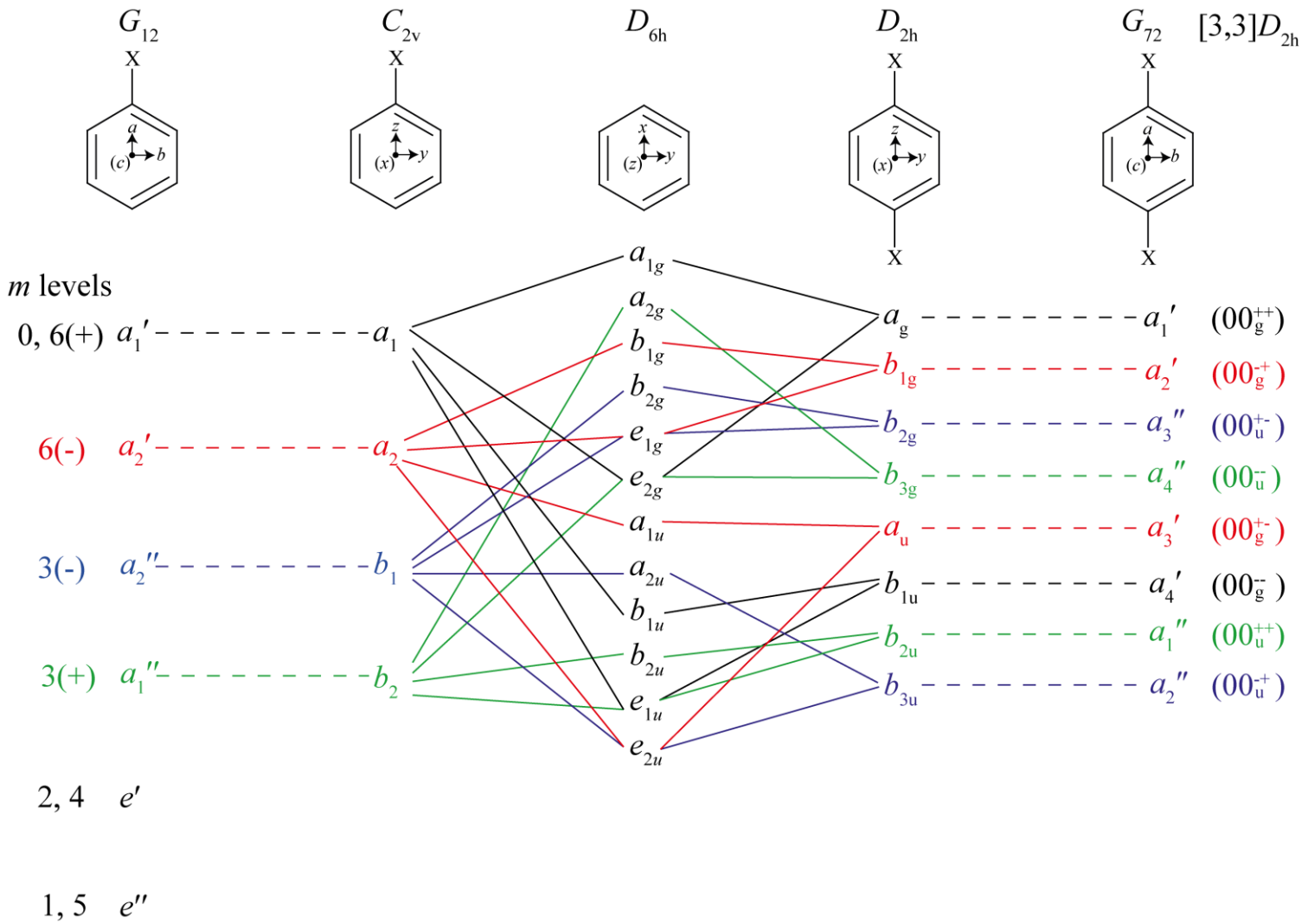
G_{12}
C_{2v}
D_{6h}
D_{2h}
G_{72}
$[3,3]D_{2h}$
X
m levels
0, 6(+) a_1' a_1
6(-) a_2' a_2
3(-) a_2'' b_1
3(+) a_1'' b_2
2, 4 e'
1, 5 e''
a_{1g} a_{2g} b_{1g} b_{2g} e_{1g} e_{2g} a_{1u} a_{2u} b_{1u} b_{2u} e_{1u} e_{2u}
a_g a_1' (00_g^{++})
b_{1g} a_2' (00_g^{-+})
b_{2g} a_3'' (00_u^{+-})
b_{3g} a_4'' (00_u^{--})
a_u a_3' (00_g^{+-})
b_{1u} a_4' (00_g^{--})
b_{2u} a_1'' (00_u^{++})
b_{3u} a_2'' (00_u^{-+})

Figure 3

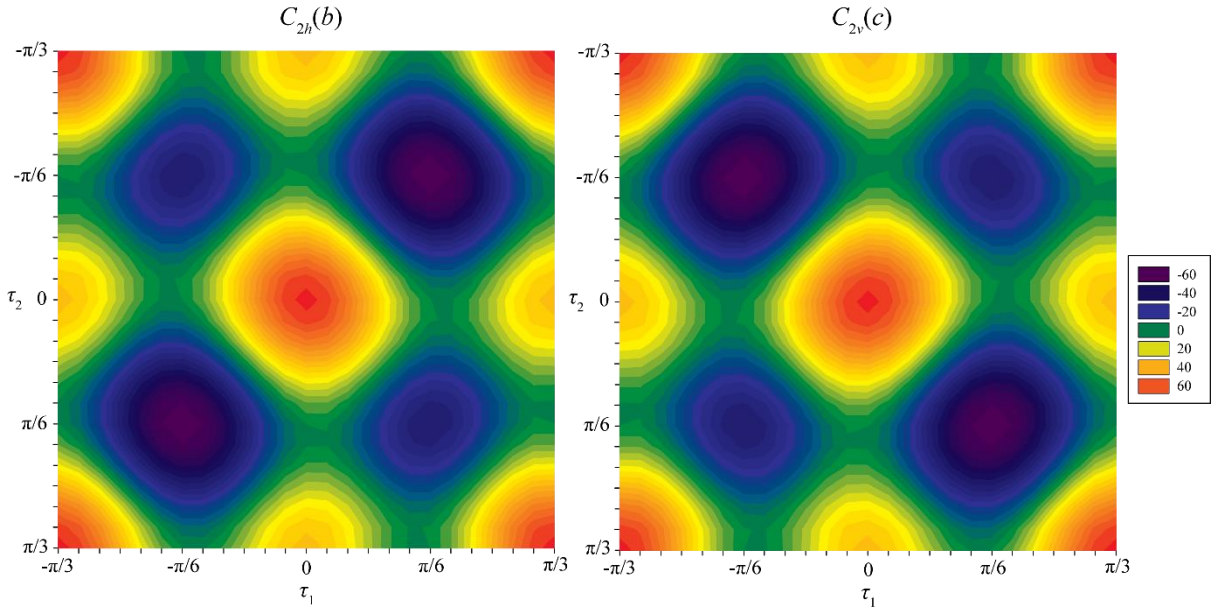

Figure 4

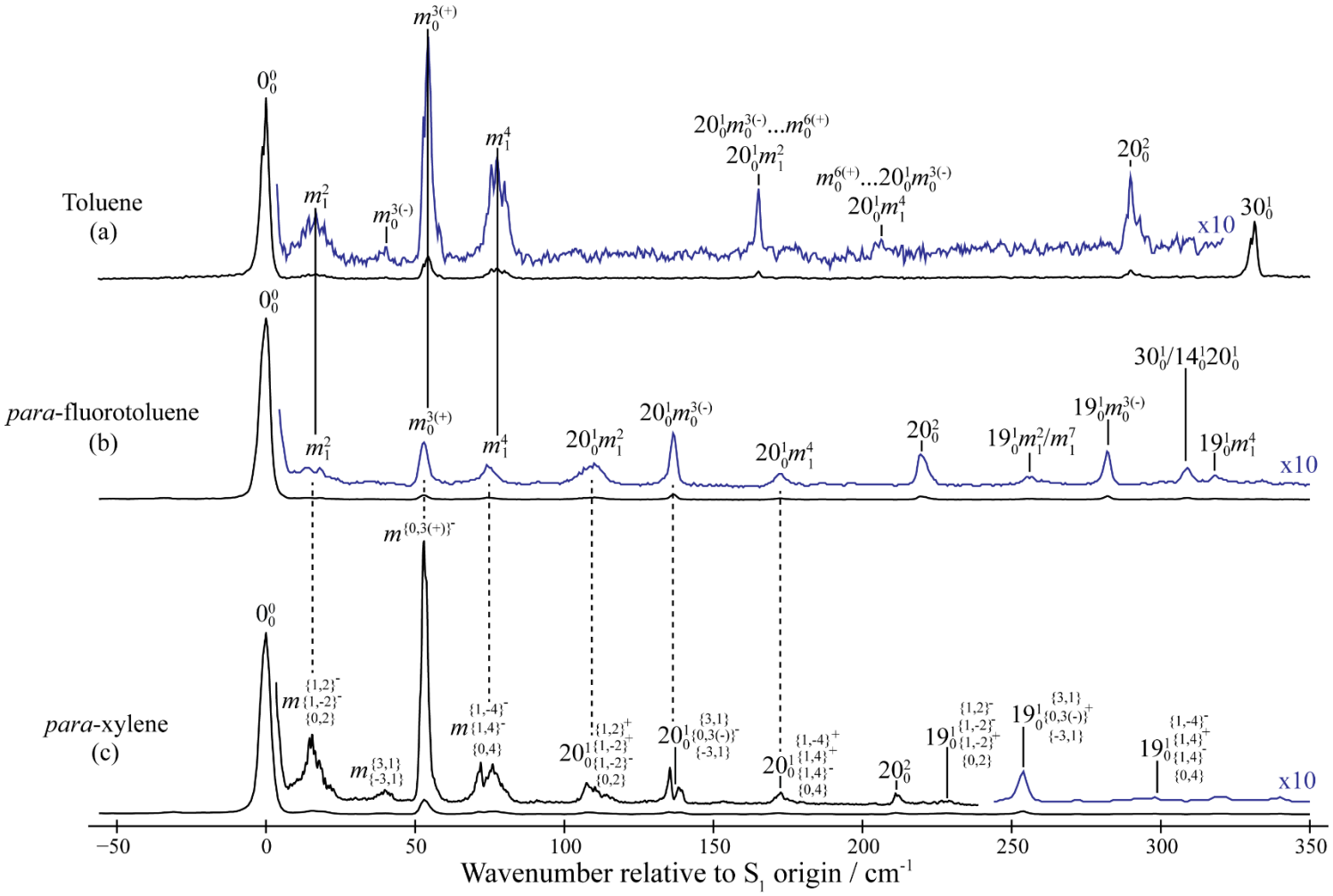
Toluene
(a)
para-fluorotoluene
(b)
para-xylene
(c)
x10
Wavenumber relative to S1 origin / cm-1

Figure 5

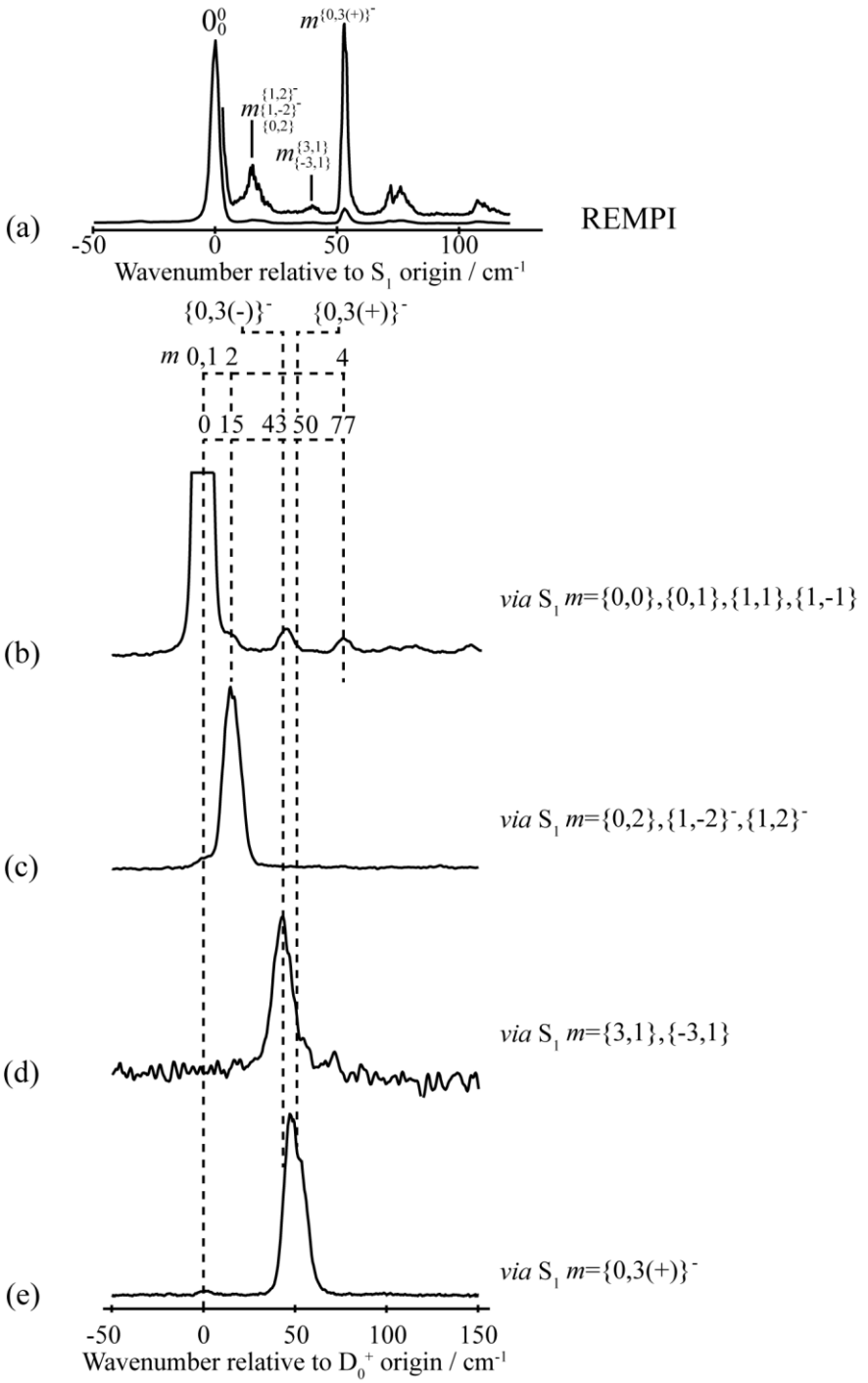
0_0^0
$m^{\{0,3(+)\}^-}$
$m^{\{1,2\}^-}_{\{1,-2\}^-}$
$m^{\{3,1\}}_{\{-3,1\}}$
(a)
REMPI
-50
0
50
100
Wavenumber relative to S_1 origin / cm^{-1}
$\{0,3(-)\}^-$
$\{0,3(+)\}^-$
m 0,1 2 4
0 15 43 50 77
(b)
via S_1 *m*={0,0},{0,1},{1,1},{1,-1}
(c)
via S_1 *m*={0,2},{1,-2}$^-$,{1,2}$^-$
(d)
via S_1 *m*={3,1},{-3,1}
(e)
via S_1 *m*={0,3(+)}$^-$
-50
0
50
100
150
Wavenumber relative to D_0^+ origin / cm^{-1}

Figure 6

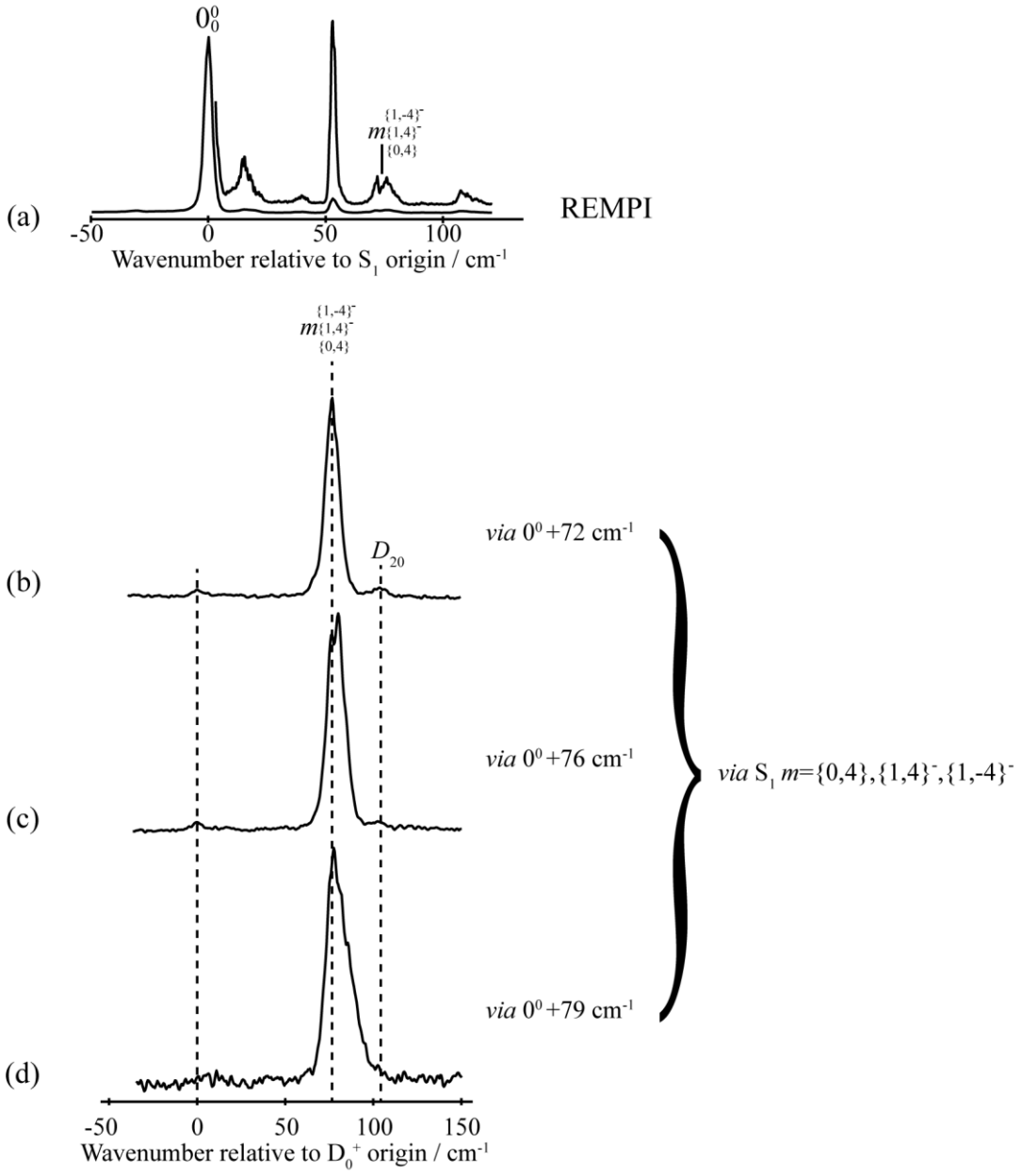
0_0^0
$m\{1,4\}^-_{\{0,4\}}$
{1,-4}-
(a)
REMPI
-50
0
50
100
Wavenumber relative to S_1 origin / cm^{-1}
$m\{1,4\}^-_{\{0,4\}}$
{1,-4}-
D_{20}
(b)
(c)
(d)
via 0^0+72 cm^{-1}
via 0^0+76 cm^{-1}
via 0^0+79 cm^{-1}
via S_1 *m*={0,4},{1,4}-,{1,-4}-
-50
0
50
100
150
Wavenumber relative to D_0^+ origin / cm^{-1}

Figure 7

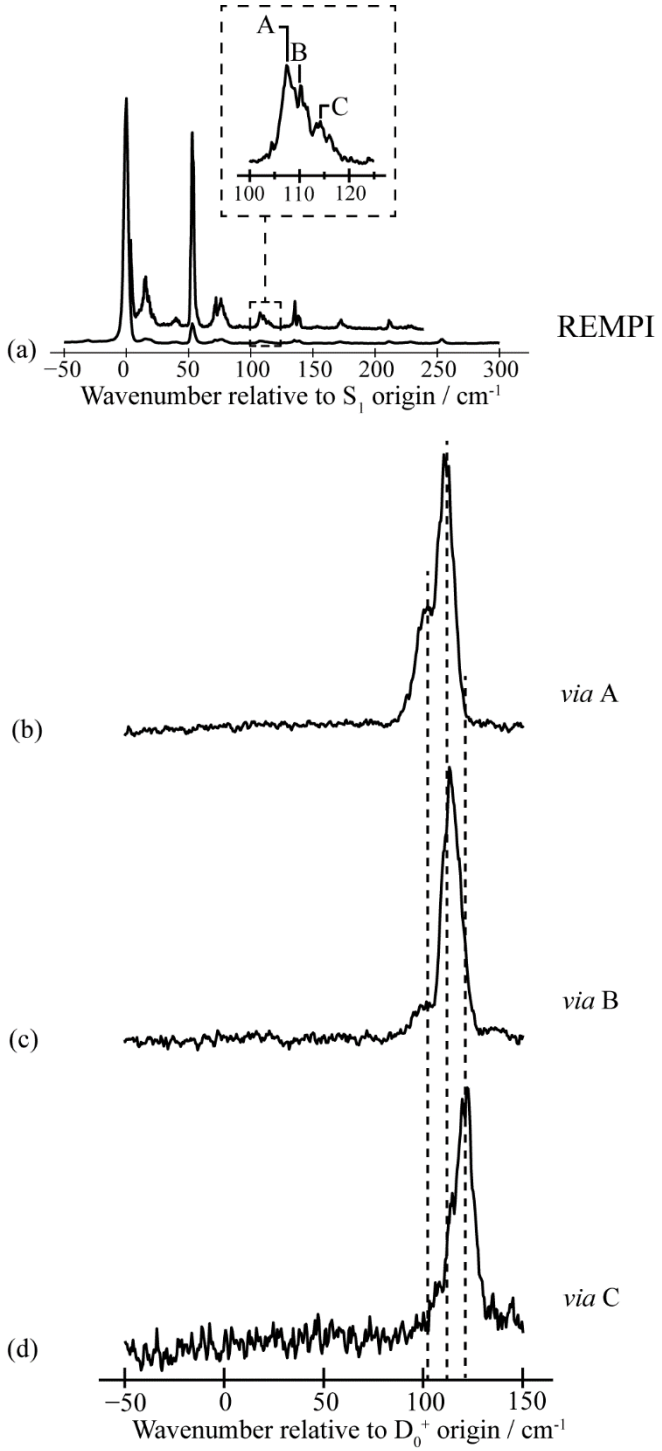
A
B
C
100 110 120
(a)
REMPI
−50 0 50 100 150 200 250 300
Wavenumber relative to S1 origin / cm-1
(b)
via A
(c)
via B
(d)
via C
−50 0 50 100 150
Wavenumber relative to D0+ origin / cm-1

Figure 8

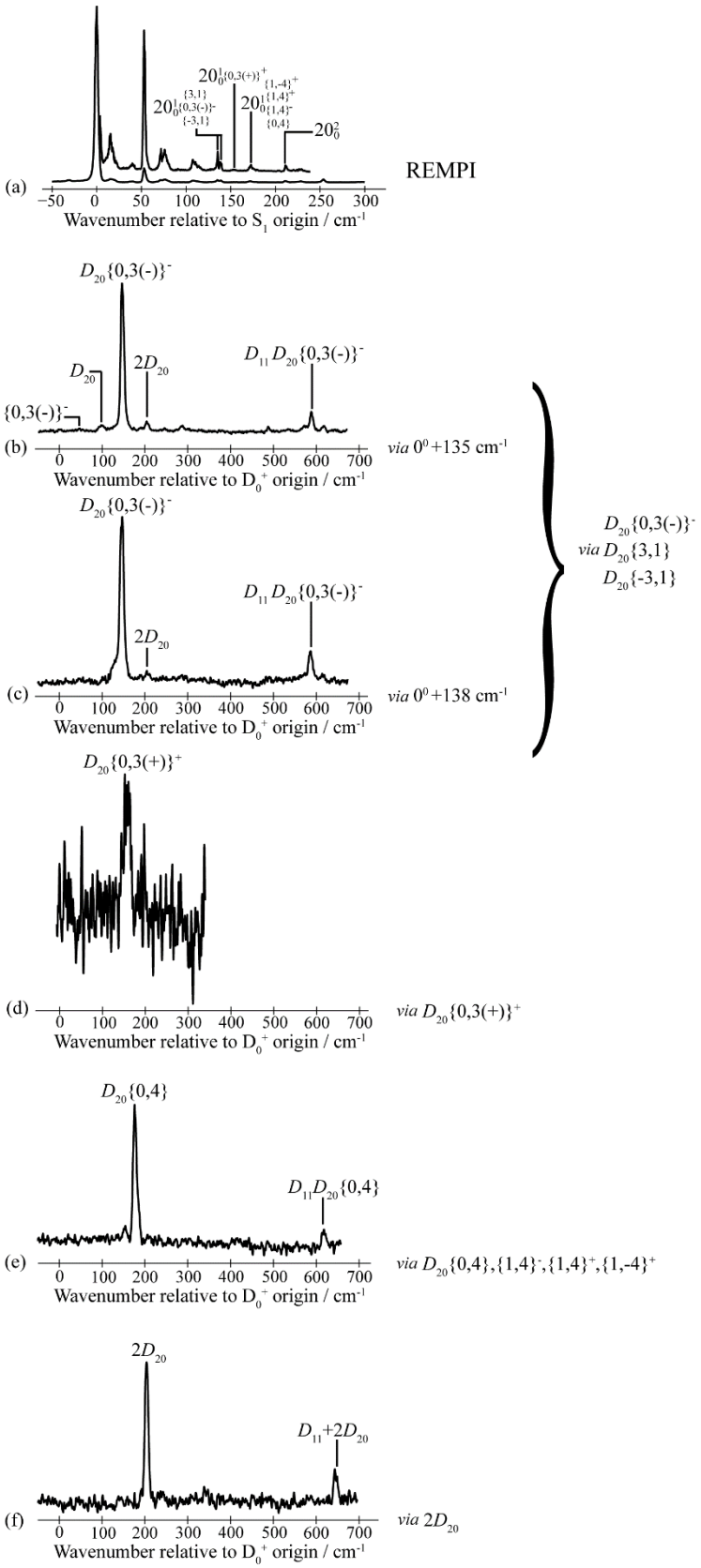
(a)
REMPI
Wavenumber relative to S1 origin / cm-1
(b)
via 0⁰ +135 cm-1
(c)
via 0⁰ +138 cm-1
D20{0,3(-)}-
via D20{3,1}
D20{-3,1}
(d)
via D20{0,3(+)}+
(e)
via D20{0,4},{1,4}-,{1,4}+,{1,-4}+
(f)
via 2D20
Wavenumber relative to D0+ origin / cm-1

Figure 9

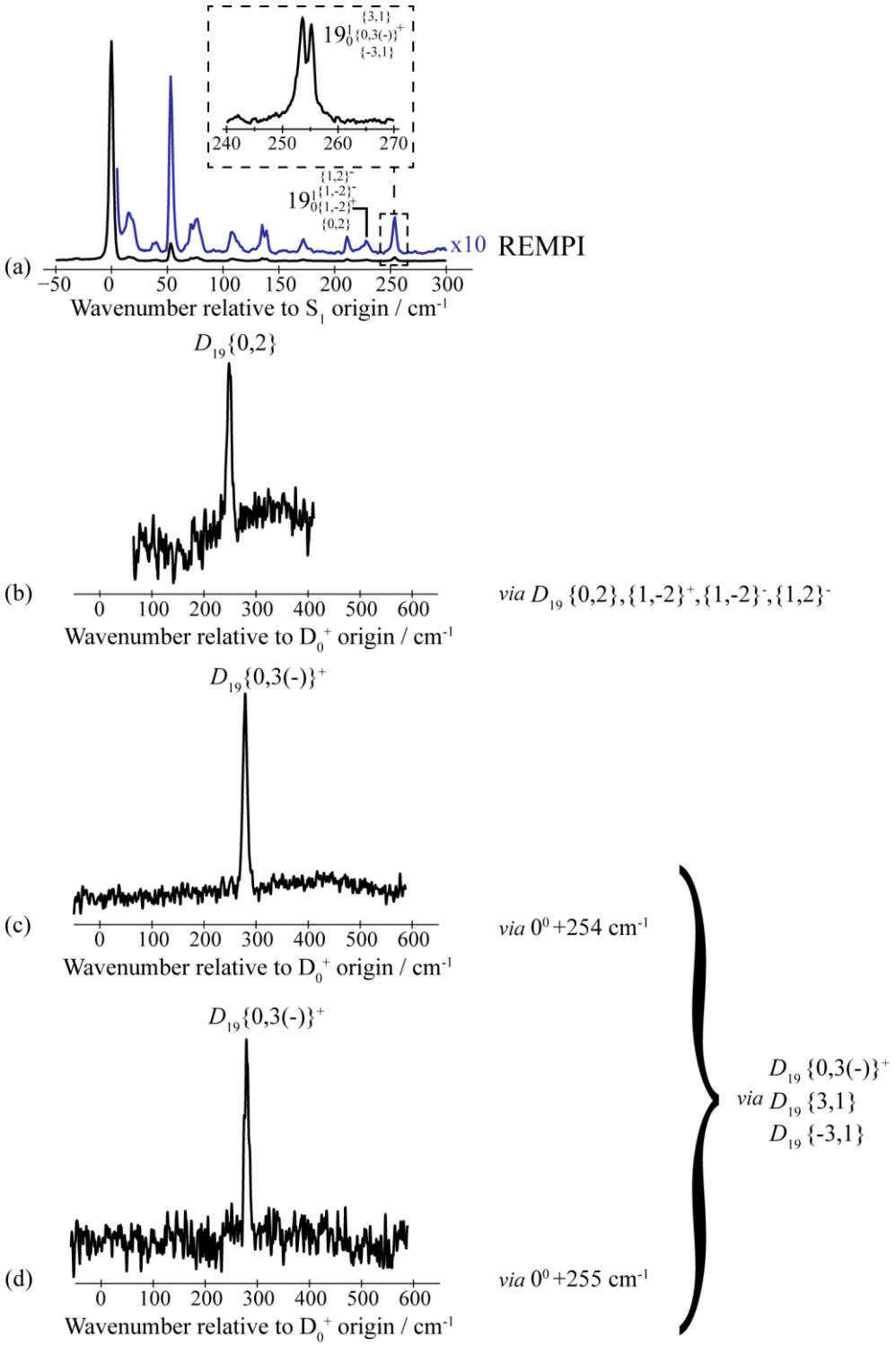
(a)
REMPI
x10
Wavenumber relative to S1 origin / cm-1
(b)
D19{0,2}
via D19 {0,2},{1,-2}+,{1,-2}-,{1,2}-
Wavenumber relative to D0+ origin / cm-1
(c)
D19{0,3(-)}+
via 0⁰+254 cm-1
Wavenumber relative to D0+ origin / cm-1
(d)
D19{0,3(-)}+
via 0⁰+255 cm-1
Wavenumber relative to D0+ origin / cm-1
D19 {0,3(-)}+
via D19 {3,1}
D19 {-3,1}

Figure 10

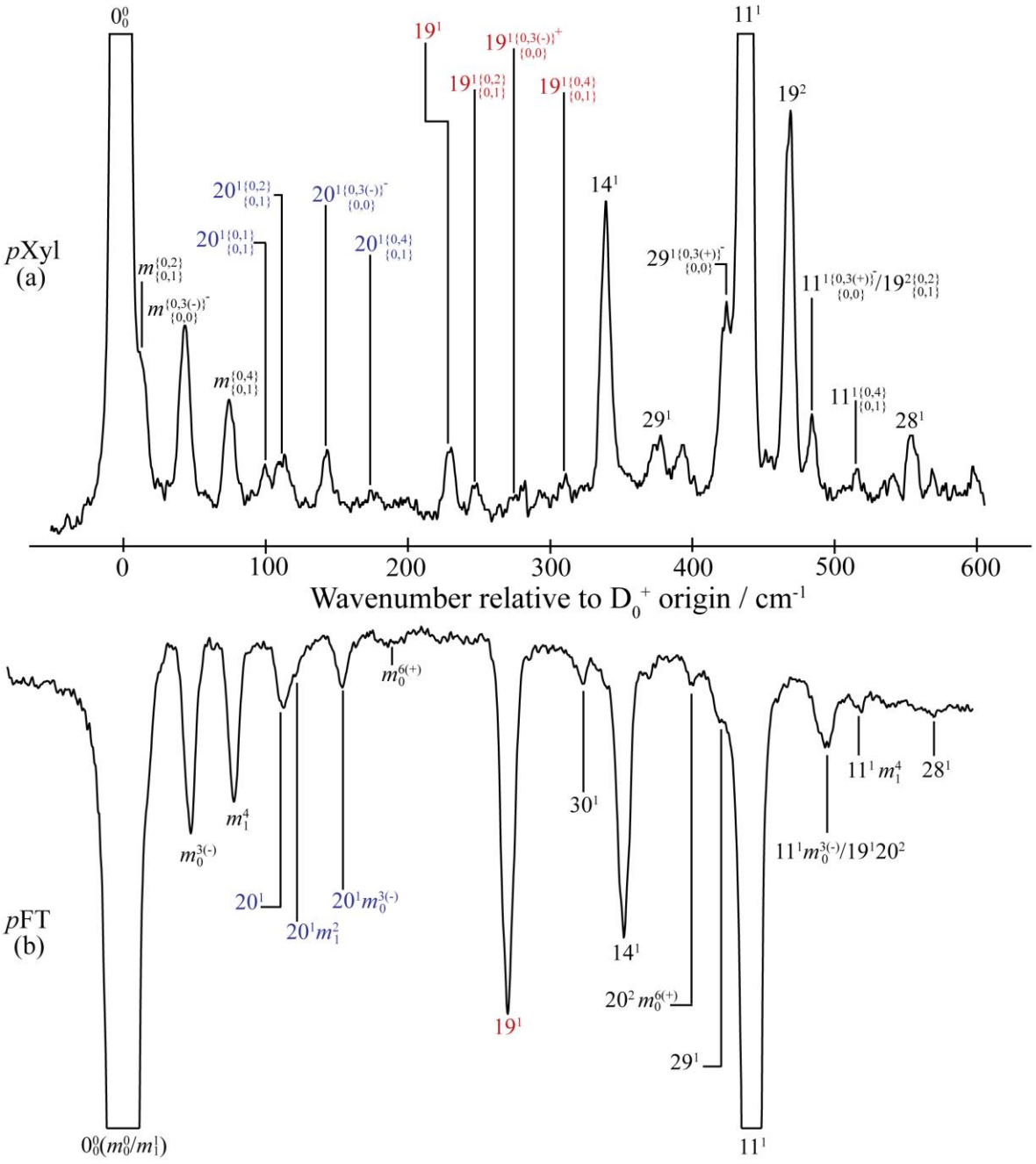
pXyl
(a)
0_0^0
19^1
$19^1\{0,3(-)\}^+_{\{0,0\}}$
$19^1\{0,2\}_{\{0,1\}}$
$19^1\{0,4\}_{\{0,1\}}$
11^1
19^2
$20^1\{0,2\}_{\{0,1\}}$
$20^1\{0,3(-)\}^-_{\{0,0\}}$
14^1
$20^1\{0,1\}_{\{0,1\}}$
$20^1\{0,4\}_{\{0,1\}}$
$29^1\{0,3(+)\}^-_{\{0,0\}}$
$m^{\{0,2\}}_{\{0,1\}}$
$11^1\{0,3(+)\}^-_{\{0,0\}}/19^2\{0,2\}_{\{0,1\}}$
$m^{\{0,3(-)\}^-}_{\{0,0\}}$
$m^{\{0,4\}}_{\{0,1\}}$
$11^1\{0,4\}_{\{0,1\}}$
29^1
28^1
0
100
200
300
400
500
600
Wavenumber relative to D_0^+ origin / cm^{-1}
pFT
(b)
$m_0^{6(+)}$
$11^1 m_1^4$
28^1
m_1^4
30^1
$m_0^{3(-)}$
$11^1 m_0^{3(-)}/19^1 20^2$
20^1
$20^1 m_0^{3(-)}$
$20^1 m_1^2$
14^1
19^1
$20^2 m_0^{6(+)}$
29^1
$0_0^0(m_0^0/m_1^1)$
11^1

References

[1] C. S. Parmenter and B. M. Stone, J. Chem. Phys. **84**, 4710 (1986).

[2] J. A. Davies and K. L. Reid, J. Chem. Phys. **135**, 124305 (2011).

[3] C. J. Hammond, V. L. Ayles, D. E. Bergeron, K. L. Reid and T. G. Wright, J. Chem. Phys. **125**, 124308 (2006)

[4] J. A. Davies, A. M. Green, A. M. Gardner, C. D. Withers, T. G. Wright, and K. L. Reid, Phys. Chem. Chem. Phys. **16**, 430 (2014).

[5] A. M. Gardner, A. M. Green, V M. Tamé-Reyes, V. H. K. Wilton and T. G. Wright J. Chem. Phys. **138**, 134303 (2013).

[6] A. M. Gardner, A. M. Green, V. M. Tamé-Reyes, K. L. Reid, J. A. Davies, V. H. K. Parkes and T. G. Wright J. Chem. Phys. **140**, 114038 (2014).

[7] J. R. Gascooke and W. D. Lawrance, J. Chem. Phys. **138**, 134302 (2013).

[8] J. R. Gascooke, E. A. Virgo and W. D. Lawrance, J. Chem. Phys. **142**, 024315 (2015).

[9] J. R. Gascooke, E. A. Virgo and W. D. Lawrance, J. Chem. Phys. **142**, 044313 (2015).

[10] Y. He, C. Wu and W. Kong, J. Phys. Chem. A **107**, 5145 (2007).

[11] C. Skinnerup Byskov, F. Jensen, T. J. D. Jørgensen, and S. Brøndsted Nielsen, Phys. Chem. Chem. Phys. **16**, 15831 (2014).

[12] V. L. Ayles, C. J. Hammond, D. E. Bergeron, O. J. Richards, and T. G. Wright J. Chem. Phys. **126** (2007), 244304.

[13] A. M. Gardner, W. D. Tuttle, L. Whalley, A. Claydon, J. H. Carter, and T. G. Wright, J. Chem. Phys **145**, 124307 (2016).

[14] L. D. Stewart, J. R. Gascooke, P. G. Sibley, and W. D. Lawrance, "Methyl torsion, low-frequency vibrations and torsion-vibration states in S_0 and S_1 *p*-fluorotoluene" (unpublished).

[15] L. D. Stewart, J. R. Gascooke, A. M. Gardner, W. D. Tuttle, T. G. Wright, and W. D. Lawrance, "Torsion-vibration interactions in the S_0 and S_1 states of *p*-fluorotoluene and the D_0^+ state of the *p*-fluorotoluene cation" (unpublished).

[16] K. Okuyama, N. Mikami and M. Ito, J. Phys. Chem. **89**, 5617 (1985).

[17] Z.-Q. Zhao, C. S. Parmenter, D. B. Moss, A. J. Bradley, A. E. W. Knight, and K. G. Owens, J. Chem. Phys. **96**, 6362 (1992).

[18] Z.-Q. Zhao, PhD Thesis, Indiana University (1992).

[19] K.-T. Lu, G. C. Eiden, and J. C. Weisshaar, J. Phys. Chem. **96**, 9742 (1992).

[20] K. Takazawa, M. Fujii, and M. Ito, J. Chem. Phys. **99**, 3205 (1993).

[21] W. D. Tuttle, A. M. Gardner, K. B. O'Regan, W. Malewicz, and T. G. Wright, J. Chem. Phys. (to be co-submitted).

[22] T. Ebata, Y. Suzuki, N. Mikami, T. Miyashi, and M. Ito, Chem. Phys. Lett. **110**, 597 (1984).

[23] P. J. Breen, J. A. Warren, E. R. Bernstein, and J. I. Seeman, J. Chem. Phys. **87**, 1917 (1987).

[24] T. G. Blease, R. J. Donovan, P. R. R. Langridge-Smith, and T. R. Ridley, Laser Chem. **9**, 241 (1988).

[25] K. Walter, K. Scherm, and U. Boesl, Chem. Phys. Lett. **161**, 473 (1989).

[26] J. I. Selco and P. G. Carrick, J Mol. Spect. **173**, 262 (1995).

[27] B. Zhang, U. Aigner, H. L. Selzle, and E. W. Schlag, Opt. Comm. **183**, 95 (2000).

[28] F. Gunzer and J. Grotemeyer, Phys. Chem. Chem. Phys. **4**, 5966 (2002).

[29] F. Gunzer and J. Grotemeyer, Int. J. Mass Spectrom. **228**, 921 (2003).

[30] B. Zhang, U. Aigner, H. L. Selzle, and E. W. Schlag, Opt. Comm. **183**, 95 (2000).

[31] A. Held, H. L. Selzle, and E. W. Schlag, J. Phys. Chem. A **102**, 9625 (1998).

[32] B. Zhang, U. Aigner, H. L. Selzle, and E. W. Schlag, Chem. Phys. Lett. **380**, 337 (2003).

[33] K. Watanabe, J. Chem. Phys. **22**, 1564 (1954).

[34] K. Watanabe, T. Nakayama, and J. Mottl, J. Quant. Spectrosc. Radiat. Transfer, **2**, 369 (1962).

[35] T. P. Debies and J. W. Rabalais, J. Electron Spect. Rel. Phenom. **1**, 355 (1972/3).

[36] M. Klessinger, Angew. Chem. Int. Ed. Engl. **11**, 525 (1972).

[37] T. Koenig, M. Tuttle, and R. A. Wielesek, Tetrahedr. Lett. **15**, 2537 (1974).

[38] J. E. Wollrab, *Rotational Spectra and Molecular Structure* (Academic Press, New York, 1967).

[39] R. A. Walker, E. Richard, K.-T. Lu, E. L. Sibert III, and J. C. Weisshaar, J. Chem. Phys. **102**, 8718 (1995).

[40] E. A. Virgo, J. R. Gascooke, and W. D. Lawrance, J. Chem. Phys. **140**, 154310 (2014).

[41] P. R. Bunker and P. Jensen, *Molecular Symmetry and Spectroscopy*, 2nd Ed. (NRCC, Ottawa, Canada, 1998).

[42] P. R. Bunker and P. Jensen, *Fundamentals of Molecular Symmetry* (Institute of Physics Publishing Ltd, London, 2005).

[43] P. Groner and J. R. Durig, J. Chem. Phys. **66**, 1856 (1977).

[44] J. T. Hougen, Can. J. Phys. **42**, 1920 (1964).

[45] P. Groner, J. Molec. Spec. **278**, 52 (2012).

[46] J. D. Swalen and C. C. Costain, J. Chem. Phys. **31**, 1562 (1959).

[47] A. E. W. Knight and S. H. Kable, J. Chem. Phys. **89**, 7139 (1988).

[48] M. R. Darafsheh and A. Darafsheh, MATCH Commun. Math. Comput. Chem. **56**, 271 (2006).

[49] Y. G. Smeyers and A. Niño, J. Comp. Chem. **8**, 380 (1987).

[50] J. Maruani, A. Hernandez-Laguna, and Y. G. Smeyers, J. Chem. Phys. **63**, 4515 (1975).

[51] J. Marauni, Y. G. Smeyers, and A. Hernández-Laguna, J. Chem. Phys. **76**, 3123 (1982).

[52] Y. G. Smeyers, J. Molec. Struct. THEOCHEM **107**, 3 (1984).

[53] Y. G. Smeyers and A. Hernández-Laguna in "Structure and Dynamics of Molecular Systems", eds. R. Daudel, J. P. Korb, J. P. Lemaister and K. Maraunipp23-240 (Dordrecht, Holland D. Reidel,1985). ISBN 9027719772/9027722463.

[54] J. T. Hougen, J. Mol. Spectrosc. **256**, 170 (2009).

[55] P. Groner, Spectrochim. Acta A **49**, 1935 (1993).

[56] R. J. Meyers and E. B. Wilson, J. Chem. Phys. **33**, 186 (1960).

[57] H. Dreizler, Z. Naturforsch. A **16**, 1354 (1961)

[58] J. R. Durig, Y. S. Li. And P. Groner, J. Mol. Spectrosc. **62**, 159 (1976).

[59] J. K. G. Watson, Can. J. Phys. **43**, 1996 (1965).

[60] P. Groner, J. Chem. Phys. **107**, 4483 (1997).

[61] A. M. Gardner and T. G. Wright, J. Chem. Phys. **135**, 114305 (2011).

[62] A. Andrejeva, A. M. Gardner, W. D. Tuttle, and T. G. Wright J. Mol. Spect. **321**, 28 (2016).

[63] S. D. Gamblin, S. E. Daire, J. Lozeille and T. G. Wright, *Chem. Phys. Lett.* 2000, **325**, 232.

[64] C. J. Hammond, V. L. Ayles, D. E. Bergeron, K. L. Reid and T. G. Wright, *J. Chem. Phys.*, 2006, **125**, 124308.

[65] X. Zhang, J. M. Smith, and J. L. Knee, J. Chem. Phys. **97**, 2843 (1992).

[66] J. P. Harris, A. Andrejeva, W. D. Tuttle, I. Pugliesi, C. Schriever, and T. G. Wright, J. Chem. Phys. **141**, 244315 (2014).

[67] A. Andrejeva, W. D. Tuttle, J. P. Harris, and T. G. Wright, J. Chem. Phys. **143**, 104312 (2015).

[68] A. Andrejeva, W. D. Tuttle, J. P. Harris, and T. G. Wright, J. Chem. Phys. **143**, 244320 (2015).

[69] W. Y. Lu, Y. H. Hu, and S. H. Yang, Z. Phys. D **40**, 40 (1997).